European Journal of Applied Mathematics (2024), 1–27
doi:10.1017/S0956792524000329

CAMBRIDGE UNIVERSITY PRESS

PAPER

Dynamical behaviour of a logarithmically sensitive chemotaxis model under time-dependent boundary conditions

Padi Fuster Aguilera[1] and Kun Zhao[2,3]

[1]Department of Mathematics, University of Colorado Boulder, Boulder, CO, USA
[2]School of Mathematical Sciences, Harbin Engineering University, Harbin, Heilongjiang Province, China, 150000
[3]Department of Mathematics, Tulane University , New Orleans, LA, 70118, USA
Corresponding author: Padi Fuster Aguilera; Email: padi.fuster@colorado.edu

Received: 20 April 2023; **Revised:** 22 April 2024; **Accepted:** 03 August 2024

Keywords: Chemotaxis; logarithmic sensitivity; dynamic boundary conditions; classical solution; global well-posedness; long-time behaviour

2020 Mathematics Subject Classification: 35Q92, 35A01, 35A02 (Primary); 35B40, 35B45, 35B65, 35M13, 65M06 (Secondary)

Abstract

This article studies the dynamical behaviour of classical solutions of a hyperbolic system of balance laws, derived from a chemotaxis model with logarithmic sensitivity, with time-dependent boundary conditions. It is shown that under suitable assumptions on the boundary data, solutions starting in the H^2-space exist globally in time and the differences between the solutions and their corresponding boundary data converge to zero as time goes to infinity. There is no smallness restriction on the magnitude of the initial perturbations. Moreover, numerical simulations show that the assumptions on the boundary data are necessary for the above-mentioned results to hold true. In addition, numerical results indicate that the solutions converge asymptotically to time-periodic states if the boundary data are time-periodic.

1. Introduction

The movement of an organism or cell in response to a chemical stimulus in its local environment is termed as chemotaxis. It is the underlying mechanism of many biological processes in modern cell biology, biochemistry and clinical pathology, such as tumour angiogenesis, blood vessel formation, slime mould formation, bacterial foraging, immune response, embryonic development, tissue homeostasis, fish pigmentation patterning, primitive streak formation, wound healing, just to mention a few. Early scholarly descriptions of chemotaxis were introduced in the late 19th century by Engelmann (1881), Pfeffer (1884), Metchnikoff (1882-1886) and Jennings (1906). Later important contributions include, but are not limited to, quality control of chemotaxis assays (Harris 1953) and study of intracellular signal transduction of bacteria (Adler 1966).

Mathematical modelling of chemotaxis using continuum partial differential equations was initiated in the 1950s by Patlak [30] from a probabilistic perspective and regained popularity in the 1970s through the seminal work of Keller and Segel [17–19] using a phenomenological approach. The original Keller–Segel models contain two prototypes according to the chemotactic sensitivity function: linear sensitivity and logarithmic sensitivity. The linear sensitivity was employed in the modelling of self-aggregation of *Dictyostelium discoideum* in response to cyclic adenosine monophosphate (cAMP) [18], while the logarithmic sensitivity appeared in [19] to interpret J. Adler's experimental result [1] on the formation of travelling bands in nutrient-enticed *E. Coli* population.

In general form, the Keller–Segel model reads as

$$u_t = Du_{xx} - \chi\left[u\Phi(c)_x\right]_x, \tag{1.1a}$$

$$c_t = \varepsilon c_{xx} - \mu u c^m - \sigma c, \tag{1.1b}$$

where the unknown functions $u(x,t)$ and $c(x,t)$ denote the density of the organism or cell population and concentration of the chemical signal at position x at time t, respectively. The parameter $D > 0$ denotes the diffusion coefficient of the organism or cell population; $\chi \neq 0$ is the coefficient of chemotactic sensitivity, the sign of χ dictates whether the chemotaxis is attractive ($\chi > 0$) or repulsive ($\chi < 0$), with $|\chi|$ measuring the strength of the chemotactic response; $\varepsilon \geq 0$ is the diffusion coefficient of the chemical signal; $\mu \neq 0$ is the coefficient of the density-dependent production/degradation rate of the chemical signal; $\sigma \geq 0$ is the natural degradation rate of the chemical signal; and $m \geq 0$ characterises the mode of temporal growth/decay of the chemical signal. Moreover, $\Phi(c)$ denotes the chemotactic sensitivity with either $\Phi(c) = c$ or $\Phi(c) = \log(c)$. The nonlinear term $-\chi\left[u\Phi(c)_x\right]_x$ underlines the main feature of (1.1), advection induced by the spatial gradient of the chemical signal in the local environment.

The pioneering work of Keller and Segel inspired many of the modern studies in chemotaxis research. From the mathematical analysis perspective, there have been studies of both of the aforementioned kinds of chemotactic sensitivity. However, a search in the literature shows that there are extensive results on the model with linear sensitivity (see e.g. [3, 12, 13]), but much less is known for the model with logarithmic sensitivity, due to its possible singular nature. The authors would like to point out that the study of the logarithmic sensitivity model is of essential importance given that this sensitivity obeys the Weber–Fechner's law, which is a fundamental principle in psychophysics and has prominent applications in biology. This article focuses on the model with logarithmic sensitivity:

$$u_t = Du_{xx} - \chi\left[u(\log c)_x\right]_x, \tag{1.2a}$$

$$c_t = \varepsilon c_{xx} - \mu u c^m - \sigma c, \tag{1.2b}$$

which has been utilised in a variety of contexts to explain the underlying mechanisms of different chemotactic processes. For example, the original Keller–Segel model ($\chi > 0$, $\mu > 0$, $0 \leq m < 1$, $\sigma = 0$) was proposed in [19] to describe the travelling bands observed in Adler's experiment [1]. The same model with $m = 1$ was employed by Levine et al [21] to interpret the dynamical interactions between vascular endothelial cells (VECs) and signalling molecules vascular endothelial growth factor (VEGF) in the onset of tumour angiogenesis. On the other hand, when $\chi < 0$, $\mu < 0$, $m = 1$ and $\sigma > 0$, the model was designed in [20, 29] to illustrate the chemotactic movement of reinforced random walkers (e.g. surface or matrix-bound adhesive molecules) that deposit non-diffusive ($\varepsilon = 0$) or slowly moving ($0 < \varepsilon \ll 1$) chemical signals that modify the local environment for succeeding passages.

Despite its versatility in biological modelling, the singular nature of the logarithmic sensitivity presents a significant challenge to both the numerical and analytical studies of the model. Depending on the value of the parameter m, the mathematical treatment of the model differs significantly. In this article, we focus on the case when $m = 1$. In this case, the singular nature can be removed by the Cole–Hopf-type transformation: $v = \frac{c_x}{c}$. By applying such a transformation and the rescalings: $t \to |\chi\mu| D^{-1} t$, $x \to \sqrt{|\chi\mu|}\, D^{-1} x$, $v \to \operatorname{sign}(\chi)\sqrt{|\chi|\,|\mu|^{-1}}\, v$, one obtains a system of conservation laws:

$$u_t - (uv)_x = u_{xx}, \tag{1.3a}$$

$$v_t - \operatorname{sign}(\chi\mu) u_x = \varepsilon D^{-1} v_{xx} + \varepsilon \chi^{-1} (v^2)_x, \tag{1.3b}$$

A direct calculation shows that the eigenvalues of the Jacobian matrix associated with the flux on the left of (1.3) are given by

$$\lambda_\pm = \frac{\left(2\varepsilon\chi^{-1} - 1\right) v \pm \sqrt{\left(2\varepsilon\chi^{-1} + 1\right)^2 v^2 + 4\operatorname{sign}(\chi\mu) u}}{2}, \tag{1.4}$$

which indicates that when $\chi\mu > 0$ and $u > 0$, the principle part of (1.3) is hyperbolic. This enables the adaptation of fundamental analytic tools in hyperbolic balance laws, such as entropy method, to study

https://doi.org/10.1017/S0956792524000329 Published online by Cambridge University Press

the qualitative behaviour of the model. Throughout this article, we focus on the case when $\chi\mu > 0$. It is worth mentioning that when $\chi\mu < 0$, the characteristic fields may change type, which could alter the dynamics of the model drastically. This is supported by the blowup (explicit and numerical) solutions constructed in [20].

Since the work of Levine and Sleeman [20], mathematical analysis of (1.3) has developed into an active area in chemotaxis research. To put things into perspective, we briefly survey the literature in connection with (1.3) when $\chi\mu > 0$. First of all, since (1.3) satisfies the Shizuta–Kawashima condition [34], the global well-posedness and stability of classical solutions to the Cauchy problem *near* constant equilibria are guaranteed by some of the contemporary frameworks on hyperbolic/parabolic balance laws (cf. [40, 41]). See also [48] for a similar result on a finite interval. For large amplitude classical solutions, the global well-posedness results on finite and infinite intervals are first established in [10] and [11], respectively. In a series of recent works [22–26, 28, 32, 35, 39], the aforementioned results are upgraded by demonstrating the *global stability* of constant equilibrium states, which suggested that uniform distribution is a generic phenomenon in logarithmically sensitive chemoattraction with chemical consumption or chemorepulsion with chemical production. In addition to the study of global dynamics, the zero chemical diffusivity limit (i.e., as $\varepsilon \to 0$) and instantaneous spatial analyticity of large amplitude classical solutions have also been investigated in [14–16, 23, 24, 28, 32, 39]. Another major direction of research is concerned with the existence and stability of non-trivial patterns of (1.3). We refer the reader to [7, 8, 31] and the references therein for the studies of large-strength travel wave solutions, and to [4–6] for non-trivial steady-state solutions. In the multi-dimensional spaces, the qualitative behaviours of the model have been investigated under various smallness assumptions on the initial data. We refer the readers to [27, 33, 37] and the references therein. Moreover, the appended version of (1.3) with logistic growth is studied in [2, 44–47] where the enhanced dissipation induced by logistic damping is explored. Furthermore, the amended model with nonlinear density-dependent chemical production/consumption rate (i.e., replacing u_x by $(u^\gamma)_x$ with $\gamma > 1$) has been analysed in [9, 49, 50].

Among the foregoing works, of particular relevance to this article is the study of the global dynamics of classical solutions to (1.3) and its companion with nonlinear chemical production/consumption rate on finite intervals subject to *time-dependent* Dirichlet boundary conditions (cf. [9, 32]). Comparing with constant valued boundary conditions, time-dependent boundary conditions are of more biological importance. For instance, nutrient availability in natural environments is often highly time-dependent. Furthermore, we note that in the previous studies, the Dirichlet boundary conditions are required to match at the endpoints of the spatial domain $I = [a, b]$, i.e., $u(a, t) = u(b, t)$, $v(a, t) = v(b, t)$. Although those results are mathematically meaningful, they are less realistic from the point of view of physical/biological applications, since, in real-world circumstances, the boundary values of certain quantity under consideration may be different time by time. Hence, mathematical studies of the model subject to *unmatching* boundary conditions becomes relevant. This is one of the motivations of this article. Moreover, (1.3) with zero chemical diffusivity (i.e., $\varepsilon = 0$) is a conceptually idealised model that was designed to simplify the underlying mathematical analysis [20]. Though such a model has been analysed under various types of boundary conditions, the large-time behaviour of classical solutions subject to time-dependent boundary conditions has never been examined.

Driven by the purpose of filling the above-mentioned gaps, we dedicate this article to study the dynamical behaviour of large-data classical solutions to (1.3) subject to time-dependent boundary conditions. First, we aim to generalise the rigorous mathematical results of [32] by studying the case of time-dependent Dirichlet boundary conditions that do not necessarily match at any time. Our goal is to identify a set of conditions on the boundary data, under which global classical solutions exist and stabilise in the long run. Second, because of the ubiquitous presence of time-periodic phenomena in nature (e.g. day/night, freeze/thaw, and rain/dry cycles) and in clinical research (e.g. administering drug delivery in cancer therapeutics [36]), we devote the second part of this article to investigate whether time-periodic boundary data induce time periodicity of the solution, and if so, how the period of the solution depends on the boundary period(s). The investigation is carried out through numerical simulations.

https://doi.org/10.1017/S0956792524000329 Published online by Cambridge University Press

The remainder of the article is organised as follows: First, we state the main analytical results in Section 2. Then, we prove the main results in Sections 3 and 4, respectively. Numerical simulations are performed in Section 5 to verify the analytical results, show that the assumptions on the boundary data are necessary for the results to hold, and study the dynamics of the solutions subject to time-periodic boundary conditions. We finish the article with concluding remarks in Section 6.

2. Statement of results

To simplify the presentation, we take $\chi = -1$, $D = 1$, since the specific values of the parameters do not affect our qualitative analysis. Also, without loss of generality, we take the spatial interval as the unit interval, i.e., $(0, 1)$. Moreover, recall that we concentrate upon the case of $\chi\mu > 0$, so $\mu < 0$. Under these circumstances, the model (1.3) is written as

$$u_t - (uv)_x = u_{xx}, \tag{2.1a}$$
$$v_t - u_x = \varepsilon v_{xx} - \varepsilon(v^2)_x. \tag{2.1b}$$

When $\varepsilon = 0$, system (2.1) becomes

$$u_t - (uv)_x = u_{xx}, \tag{2.2a}$$
$$v_t - u_x = 0. \tag{2.2b}$$

Both (2.1) and (2.2) are subject to the initial condition

$$(u, v)(x, 0) = (u_0, v_0)(x), \quad x \in [0, 1]. \tag{2.3}$$

When $\varepsilon > 0$, (2.1) is supplemented with the boundary conditions:

$$u(0, t) = \alpha_1(t), \quad u(1, t) = \alpha_2(t), \quad t \geq 0, \tag{2.4a}$$
$$v(0, t) = \beta_1(t), \quad v(1, t) = \beta_2(t), \quad t \geq 0. \tag{2.4b}$$

When $\varepsilon = 0$, only the function u needs supplementary information from the boundary:

$$u(0, t) = \alpha_1(t), \quad u(1, t) = \alpha_2(t), \quad t \geq 0, \tag{2.5}$$

while the function v does not, since otherwise the system would be over-determined.

With the initial and boundary conditions at our disposal, we are now ready to present the main results of this paper. The first one is concerned with the global nonlinear stability of large-data classical solutions to the diffusive model under unmatching dynamic boundary conditions for v. This upgrades the result of [32], where the case of matching boundary data is analysed.

Theorem 2.1. *Consider the initial-boundary value problem (2.1), (2.3), (2.4). Suppose the initial data satisfy $u_0 > 0$, $(u_0, v_0) \in [H^2((0, 1))]^2$ and are compatible with the boundary conditions. Assume $\alpha_1 = \alpha_2 = \alpha$, β_1 and β_2 are smooth functions on $[0, \infty)$ satisfying*

- $\alpha(t) \geq \underline{\alpha} > 0, \quad \forall\, t \geq 0, \quad$ *and* $\quad \alpha' \in W^{1,1}(\mathbb{R}_+),$ (2.6)
- $\beta_1 - \beta_2 \in L^1(\mathbb{R}_+) \quad$ *and* $\quad \beta_1', \beta_2' \in W^{1,1}(\mathbb{R}_+),$ (2.7)

where $\underline{\alpha}$ is a constant. Then, there exists a unique solution to the IBVP such that

$$\|\tilde{u}(t)\|^2_{H^2((0,1))} + \|\tilde{v}(t)\|^2_{H^2((0,1))} + \int_0^t \big(\|\tilde{u}(\tau)\|^2_{H^3((0,1))} + \|\tilde{v}(\tau)\|^2_{H^3((0,1))}\big)\mathrm{d}\tau \leq C,$$

where $\tilde{u}(x, t) = u(x, t) - \alpha(t)$, $\tilde{v}(x, t) = v(x, t) - [\beta_2(t) - \beta_1(t)]x - \beta_1(t)$, and the constant $C > 0$ is independent of t. Moreover, the solution has the large-time behaviour:

$$\|\tilde{u}(t)\|_{H^2((0,1))} + \|\tilde{v}(t)\|_{H^2((0,1))} \to 0 \quad as \quad t \to \infty.$$

The second theorem addresses the dynamics of large-data classical solutions to the non-chemically-diffusive model subject to matching dynamic boundary conditions for u, which has not been documented

https://doi.org/10.1017/S0956792524000329 Published online by Cambridge University Press

in the literature. This is a generalisation of the result of [23, 24], where the global stability of constant Dirichlet-type boundary condition is established.

Theorem 2.2. *Consider the initial-boundary value problem* (2.2), (2.3), (2.5). *Suppose the initial data satisfy* $u_0 > 0$, $(u_0, v_0) \in [H^2((0,1))]^2$ *and are compatible with the boundary conditions. Assume* $\alpha_1 = \alpha_2 = \alpha$ *is a smooth function on* $[0, \infty)$ *satisfying*

$$\alpha(t) \geq \underline{\alpha} > 0, \quad \forall\, t \geq 0, \quad \text{and} \quad \alpha' \in W^{1,1}(\mathbb{R}_+),$$

where $\underline{\alpha}$ *is a constant. Then, there exists a unique solution to the IBVP such that*

$$\|\tilde{u}(t)\|^2_{H^2((0,1))} + \|\tilde{v}(t)\|^2_{H^2((0,1))} + \int_0^t \left(\|\tilde{u}(\tau)\|^2_{H^3((0,1))} + \|\tilde{v}(\tau)\|^2_{H^2((0,1))}\right)\mathrm{d}\tau \leq C,$$

where $\tilde{u}(x,t) = u(x,t) - \alpha(t)$, $\tilde{v}(x,t) = v(x,t) - \int_0^1 v_0(x)\mathrm{d}x$, *and the constant* $C > 0$ *is independent of* t. *Moreover, the solution has the large-time behaviour:*

$$\|\tilde{u}(t)\|_{H^2((0,1))} + \|\tilde{v}(t)\|_{H^2((0,1))} \to 0 \quad \text{as} \quad t \to \infty.$$

We have several remarks concerning Theorems 2.1 and 2.2.

Remark 2.1. *The assumptions in Theorem* 2.1 *imply that the difference between* $\beta_1(t)$ *and* $\beta_2(t)$ *will converge to zero as* $t \to \infty$, *i.e., the unmatching boundary data will eventually match. However, based on the assumptions, we see that the boundary functions are not necessarily equal to each other at any finite time. This generalises all of the previous results for the model under matching boundary conditions. We also expect that our results will help provide useful information for the understanding of more realistic situations involving logarithmically sensitive chemotaxis.*

Remark 2.2. *Since the boundary functions are smooth on* $[0, \infty)$ *and their first order derivatives belong to* $W^{1,1}(\mathbb{R}_+)$, *it follows from the Fundamental Theorem of Calculus that the functions themselves alongside their first-order derivatives are uniformly bounded with respect to* t. *Such information will be frequently utilized in the proof of the theorems.*

Remark 2.3. *It is an intriguing question to ask whether the matching boundary data of* u *can be relaxed, i.e.,* $\alpha_1(t) \neq \alpha_2(t)$. *In this case, the reference profile interpolating the boundary values becomes* $\alpha_1(t) + x[\alpha_2(t) - \alpha_1(t)]$. *Unfortunately, the* x*-dependence of the profile picks up additional nonlinearities when implementing the entropy estimate, see* (3.2), *which cannot be handled by using the approach in this paper, due to the sub-quadraticity of the relative entropy. We leave the investigation for the future.*

Remark 2.4. *Theorem* 2.1 *suggests that the large-time behaviour of* (2.1) *is determined by its boundary data, while its initial information is gradually lost as time evolves. On the other hand, Theorem* 2.2 *indicates that both its initial and boundary information are carried by* (2.2) *in the long run. It is interesting to investigate whether there are mechanisms that can drive the solutions to other stationary solutions rather than those determined by the initial and/or boundary data. Among various types of modelling structures, the logistic growth may give us a definite answer. However, the analysis in this paper can not be directly carried over to the model with logistic growth, due to the quadratic nonlinearity. We will report such a result in a forthcoming paper.*

Remark 2.5. *Systems* (2.1) *and* (2.2) *themselves have deep mathematical interests as they serve as prototypes of general parabolic/hyperbolic balance laws. The nature of possible non-uniform dissipativity (i.e.,* $\varepsilon = 0$*) coupled with nonlinear flux functions, together with the non-triviality of the dynamic boundary data in this type of problems, presents significant challenges in mathematical analysis. The analysis of* (2.1) *and* (2.2) *helps to shed light on how to advance fundamental research of parabolic/hyperbolic balance laws in related topics, and we expect the study in this paper to be helpful to other parabolic/hyperbolic balance laws.*

https://doi.org/10.1017/S0956792524000329 Published online by Cambridge University Press

We prove Theorem 2.1 and Theorem 2.2 in Section 3 and Section 4, respectively. The integrability conditions of the boundary data are thoroughly examined to fit into the framework previously established for the case of matching boundary conditions. The proof of Theorem 2.1 takes advantage of the fully dissipative structure of (2.1), which results in energy estimates depending on the reciprocal of the chemical diffusion coefficient. For this reason, the arguments cannot be carried over to (2.2). Instead, Theorem 2.2 is proven by deriving a nonlinear damping equation for the spatial derivative of v. It should be mentioned that the approach for analysing (2.2) cannot be utilised for (2.1), due to the lack of information of higher order spatial derivatives of the solution to the latter, causing integration-by-parts to be unaccessible. Thus, the energy methods for studying (2.1) and (2.2) are mutually exclusive.

Lastly, for notational convenience, throughout the rest of the article, we use $\|\cdot\|$, $\|\cdot\|_{H^s}$ and $\|\cdot\|_\infty$ to denote the standard norms $\|\cdot\|_{L^2((0,1))}$, $\|\cdot\|_{H^s((0,1))}$ and $\|\cdot\|_{L^\infty((0,1))}$, respectively. Moreover, we use C to denote a generic constant which is independent of time, but may depend on the parameter ε and initial and/or boundary data. The value of the constant may vary line by line according to the context.

3. Proof of Theorem 2.1

The proof of Theorem 2.1 is divided into five steps contained in five subsections. First of all, the local well-posedness of the IBVP under the assumptions of Theorem 2.1 can be established via standard approaches, such as mollification, Galerkin approximation, energy estimate, contraction mapping principle and compactness argument. We omit most of the standard technical details for brevity, while focus on deriving the *a priori* estimates of the local solution, in order to extend it to a global one. The *a priori* estimates can be justified by standard means, which are indeed carried out on the local smooth approximate solutions obtained from the mollified initial data and contraction mapping. Moreover, according to the assumptions in Theorem 2.1 and the maximum principle, the local solution u is positive within its life span, say, $[0, T^*)$ for some $T^* > 0$. The subsequent estimates are derived within such a time window. It will be shown that the estimates are indeed independent of t. Then, the global well-posedness follows from the uniform estimates and standard continuation argument. We begin with an estimate based on the relative entropy-entropy flux pair associated with the IBVP.

3.1. Entropy estimate

Lemma 3.1. *Under the assumptions of Theorem 2.1, there exists a constant $C > 0$ which is independent of t, such that*

$$E(u,\alpha)(t) + \|(v-\beta)(t)\|^2 + \int_0^t \int_0^1 \frac{(u_x)^2}{u}\mathrm{d}x\mathrm{d}\tau + \int_0^t \varepsilon\|(v_x-\beta_x)(\tau)\|^2\mathrm{d}\tau \le C,$$

where $\beta(x,t) = [\beta_2(t) - \beta_1(t)]x + \beta_1(t)$ and

$$E(u,\alpha) \equiv \int_0^1 [(u\ln u - u) - (\alpha\ln\alpha - \alpha) - (u-\alpha)\ln\alpha]\,\mathrm{d}x \ge 0$$

denotes the relative entropy.

Proof. Step 1. By a direct calculation, we can show that

$$(u\ln u - u)_t - (\alpha\ln\alpha - \alpha)_t - [(u-\alpha)\ln\alpha]_t = (\ln u - \ln\alpha)u_t - (u-\alpha)\frac{\alpha'}{\alpha}. \tag{3.1}$$

Using equation (2.1a) and noting α depends only on t, we deduce

$$(\ln u - \ln\alpha)u_t = [(\ln u - \ln\alpha)uv]_x + [(\ln u - \ln\alpha)u_x]_x - v\,u_x - \frac{(u_x)^2}{u}. \tag{3.2}$$

https://doi.org/10.1017/S0956792524000329 Published online by Cambridge University Press

Substituting (3.2) into (3.1) gives us

$$\begin{aligned}&(u\ln u-u)_t-(\alpha\ln\alpha-\alpha)_t-[(u-\alpha)\ln\alpha]_t\\&=[(\ln u-\ln\alpha)uv]_x+[(\ln u-\ln\alpha)u_x]_x-vu_x-\frac{(u_x)^2}{u}-(u-\alpha)\frac{\alpha'}{\alpha}.\end{aligned}\tag{3.3}$$

Integrating (3.3) over [0, 1] and using the boundary conditions, we have

$$\frac{\mathrm{d}}{\mathrm{d}t}E(u,\alpha)+\int_0^1\frac{(u_x)^2}{u}\mathrm{d}x=-\int_0^1 vu_x\mathrm{d}x-\int_0^1(u-\alpha)\frac{\alpha'}{\alpha}\mathrm{d}x.\tag{3.4}$$

Let $\beta(x,t)=[\beta_2(t)-\beta_1(t)]x+\beta_1(t)$. Then, we derive from equation (2.1b) that

$$\begin{aligned}&(v-\beta)_t-u_x\\&=\varepsilon(v-\beta)_{xx}-2\varepsilon(v-\beta)(v-\beta)_x-2\varepsilon(v-\beta)\beta_x-2\varepsilon\beta(v-\beta)_x-2\varepsilon\beta\beta_x-\beta_t.\end{aligned}\tag{3.5}$$

Taking L^2 inner product of (3.5) with $v-\beta$ and using the boundary conditions, we obtain

$$\begin{aligned}&\frac{1}{2}\frac{\mathrm{d}}{\mathrm{d}t}\|v-\beta\|^2+\varepsilon\|(v-\beta)_x\|^2\\&=\int_0^1(v-\beta)u_x\mathrm{d}x-\varepsilon\int_0^1(v-\beta)^2\beta_x\mathrm{d}x-2\varepsilon\int_0^1\beta\beta_x(v-\beta)\mathrm{d}x-\int_0^1(v-\beta)\beta_t\mathrm{d}x.\end{aligned}\tag{3.6}$$

Note since α is independent of x, it holds that

$$\int_0^1(v-\beta)u_x\mathrm{d}x=\int_0^1 vu_x\mathrm{d}x+\int_0^1\beta_x(u-\alpha)\mathrm{d}x.$$

We then get from (3.6) that

$$\begin{aligned}\frac{1}{2}\frac{\mathrm{d}}{\mathrm{d}t}\|v-\beta\|^2+\varepsilon\|(v-\beta)_x\|^2=&\int_0^1 vu_x\mathrm{d}x+\int_0^1\beta_x(u-\alpha)\mathrm{d}x-\varepsilon\int_0^1(v-\beta)^2\beta_x\mathrm{d}x\\&-2\varepsilon\int_0^1\beta\beta_x(v-\beta)\mathrm{d}x-\int_0^1(v-\beta)\beta_t\mathrm{d}x.\end{aligned}\tag{3.7}$$

Adding (3.7) and (3.4), we can show that

$$\begin{aligned}&\frac{\mathrm{d}}{\mathrm{d}t}\Big(E(u,\alpha)+\frac{1}{2}\|v-\beta\|^2\Big)+\int_0^1\frac{(u_x)^2}{u}\mathrm{d}x+\|(v-\beta)_x\|^2\\&=\int_0^1(u-\alpha)\Big(\beta_x-\frac{\alpha'}{\alpha}\Big)\mathrm{d}x-\varepsilon\int_0^1(v-\beta)^2\beta_x\mathrm{d}x-\int_0^1(2\varepsilon\beta\beta_x+\beta_t)(v-\beta)\mathrm{d}x\\&\le\Big(\frac{|\alpha'|}{\alpha}+|\beta_x|\Big)\int_0^1|u-\alpha|\mathrm{d}x+\varepsilon|\beta_x|\,\|\beta-v\|^2+\int_0^1\big(2\varepsilon|\beta\beta_x|+|\beta_t|\big)|v-\beta|\mathrm{d}x.\end{aligned}\tag{3.8}$$

Step 2. Define

$$F_\alpha(u)\equiv(u\ln u-u)-(\alpha\ln\alpha-\alpha)-(u-\alpha)\ln\alpha+(e-1)\alpha-u.$$

Then, it can be readily checked that $F_\alpha(e\alpha)=0$, $F'_\alpha(e\alpha)=0$, and $F''_\alpha(u)=\frac{1}{u}\ge 0$ for $u\ge 0$. These imply $F_\alpha(u)\ge 0$ for $u\ge 0$. Hence,

$$0\le u\le(u\ln u-u)-(\alpha\ln\alpha-\alpha)-(u-\alpha)\ln\alpha+(e-1)\alpha,$$

which yields

$$0\le\int_0^1 u(x,t)\mathrm{d}x\le E(u,\alpha)+(e-1)\alpha.\tag{3.9}$$

The triangle inequality then gives us

$$\int_0^1|u-\alpha|\mathrm{d}x\le E(u,\alpha)+e\alpha.\tag{3.10}$$

https://doi.org/10.1017/S0956792524000329 Published online by Cambridge University Press

Applying (3.10) to the right-hand side of (3.8), we can show that

- $\left(\frac{|\alpha'|}{\alpha}+|\beta_x|\right)\int_0^1 |u-\alpha|\mathrm{d}x \le C\big(|\alpha'|+|\beta_1-\beta_2|\big)\big[E(u,\alpha)+1\big]$,
- $\varepsilon|\beta_x|\,\|\beta-v\|^2 \le \varepsilon|\beta_1-\beta_2|\,\|\beta-v\|^2$,
- $\int_0^1 \big(2\varepsilon|\beta\beta_x|+|\beta_t|\big)|v-\beta|\mathrm{d}x \le C\big(\varepsilon|\beta_1-\beta_2|+|\beta_1'|+|\beta_2'|\big)\big(\|v-\beta\|^2+1\big)$,

where we used the uniform boundedness of β and the Cauchy–Schwarz inequality. Using the above estimates, we update (3.8) as

$$\begin{aligned}&\frac{\mathrm{d}}{\mathrm{d}t}\Big(E(u,\alpha)+\frac{1}{2}\|v-\beta\|^2+1\Big)+\int_0^1\frac{(u_x)^2}{u}\mathrm{d}x+\varepsilon\|(v-\beta)_x\|^2\\ &\le C\big(|\alpha'|+\varepsilon|\beta_1-\beta_2|+|\beta_1'|+|\beta_2'|\big)\Big(E(u,\alpha)+\frac{1}{2}\|v-\beta\|^2+1\Big).\end{aligned}\tag{3.11}$$

Applying Grönwall's inequality to (3.11) and using the assumptions in Theorem 2.1 give us

$$E(u,\alpha)(t)+\frac{1}{2}\|(v-\beta)(t)\|^2\le C.\tag{3.12}$$

Substituting (3.12) into (3.11), then integrating with respect to t, we have in particular,

$$\int_0^t\int_0^1\frac{(u_x)^2}{u}\mathrm{d}x\mathrm{d}\tau+\int_0^t\varepsilon\|(v_x-\beta_x)(\tau)\|^2\mathrm{d}\tau\le C,\tag{3.13}$$

where the constant is independent of t. This, along with (3.12), completes the proof of Lemma 3.1. □

3.2. $L_t^\infty L_x^2$–$L_t^2 H_x^1$–estimates

We now switch to standard L^2-based energy estimates. To facilitate our asymptotic analysis, we define

$$\tilde{u}\equiv u-\alpha\quad\text{and}\quad\tilde{v}\equiv v-\beta,$$

where (u,v) satisfies (2.1) and $\beta(x,t)=[\beta_2(t)-\beta_1(t)]x+\beta_1(t)$. Then, $(\tilde{u},\tilde{v})$ satisfies

$$\tilde{u}_t-(\tilde{u}\tilde{v})_x=\tilde{u}_{xx}+\alpha\tilde{v}_x+\beta\tilde{u}_x+\beta_x\tilde{u}+\alpha\beta_x-\alpha',\tag{3.14a}$$

$$\tilde{v}_t-\tilde{u}_x=\varepsilon\tilde{v}_{xx}-2\varepsilon\tilde{v}\tilde{v}_x-2\varepsilon\beta\tilde{v}_x-2\varepsilon\tilde{v}\beta_x-2\varepsilon\beta\beta_x-\beta_t,\tag{3.14b}$$

$$(\tilde{u},\tilde{v})(x,0)=(u_0(x)-\alpha(0),v_0(x)-\beta(x,0)),\tag{3.14c}$$

$$\tilde{u}(0,t)=\tilde{u}(1,t)=0,\quad\tilde{v}(0,t)=\tilde{v}(1,t)=0.\tag{3.14d}$$

Using Lemma 3.1, we can show the following:

Lemma 3.2. *Under the assumptions of Theorem 2.1, there exists a constant $C>0$ which is independent of t, such that*

$$\|\tilde{u}(t)\|^2+\|\tilde{v}(t)\|^2+\int_0^t\|\tilde{u}_x(\tau)\|^2\mathrm{d}\tau\le C.$$

Proof. Step 1. Taking L^2 inner product of (3.14a) with $\tilde{u}$, we have

$$\frac{1}{2}\frac{\mathrm{d}}{\mathrm{d}t}\|\tilde{u}\|^2+\|\tilde{u}_x\|^2=-\int_0^1\tilde{u}\tilde{v}\tilde{u}_x\mathrm{d}x+\alpha\int_0^1\tilde{u}\tilde{v}_x\mathrm{d}x+(\alpha\beta_x-\alpha')\int_0^1\tilde{u}\mathrm{d}x+\frac{\beta_x}{2}\|\tilde{u}\|^2.\tag{3.15}$$

https://doi.org/10.1017/S0956792524000329 Published online by Cambridge University Press

Taking L^2 inner product of (3.14b) with $\tilde{v}$ yields

$$\frac{1}{2}\frac{\mathrm{d}}{\mathrm{d}t}\|\tilde{v}\|^2+\varepsilon\|\tilde{v}_x\|^2=\int_0^1\tilde{v}\tilde{u}_x\mathrm{d}x-\varepsilon\beta_x\|\tilde{v}\|^2-\int_0^1(2\varepsilon\beta\beta_x+\beta_t)\tilde{v}\mathrm{d}x. \tag{3.16}$$

Multiplying (3.16) by α, we obtain

$$\frac{1}{2}\frac{\mathrm{d}}{\mathrm{d}t}\left(\alpha\|\tilde{v}\|^2\right)+\alpha\varepsilon\|\tilde{v}_x\|^2=-\alpha\int_0^1\tilde{u}\tilde{v}_x\mathrm{d}x+\left(\frac{\alpha'}{2}-\alpha\varepsilon\beta_x\right)\|\tilde{v}\|^2-\alpha\int_0^1(2\varepsilon\beta\beta_x+\beta_t)\tilde{v}\mathrm{d}x. \tag{3.17}$$

Adding (3.17) to (3.15) gives us

$$\begin{aligned}\frac{1}{2}\frac{\mathrm{d}}{\mathrm{d}t}\left(\|\tilde{u}\|^2+\alpha\|\tilde{v}\|^2\right)+\|\tilde{u}_x\|^2+\alpha\varepsilon\|\tilde{v}_x\|^2=&-\int_0^1\tilde{u}\tilde{v}\tilde{u}_x\mathrm{d}x+(\alpha\beta_x-\alpha')\int_0^1\tilde{u}\mathrm{d}x+\frac{\beta_x}{2}\|\tilde{u}\|^2\\&+\left(\frac{\alpha'}{2}-\alpha\varepsilon\beta_x\right)\|\tilde{v}\|^2-\alpha\int_0^1(2\varepsilon\beta\beta_x+\beta_t)\tilde{v}\mathrm{d}x\equiv\sum_{k=1}^5 I_k.\end{aligned} \tag{3.18}$$

Step 2. To estimate I_1, we note that

$$|I_1|\le\frac{1}{2}\|\tilde{u}\|_{L^\infty}^2\|\tilde{v}\|^2+\frac{1}{2}\|\tilde{u}_x\|^2\le C\|\tilde{u}\|_{L^\infty}^2+\frac{1}{2}\|\tilde{u}_x\|^2, \tag{3.19}$$

where we used (3.12). Since $\tilde{u}(0,t)=0$, for any $x\in[0,1]$, it holds that

$$|\tilde{u}(x,t)|^2=\left|\int_0^x\tilde{u}_y(y,t)\mathrm{d}y\right|^2\le\left(\int_0^1|\tilde{u}_x|\mathrm{d}x\right)^2\le\left(\int_0^1u(x,t)\mathrm{d}x\right)\left(\int_0^1\frac{(\tilde{u}_x)^2}{u}\mathrm{d}x\right), \tag{3.20}$$

where u denotes the solution to (2.1). Since $E(u,\alpha)$ and α are uniformly bounded with respect to t (see (3.12)), we obtain from (3.9) and (3.20) that

$$\|\tilde{u}(t)\|_{L^\infty}^2\le C\int_0^1\frac{(\tilde{u}_x)^2}{u}\mathrm{d}x. \tag{3.21}$$

Substituting (3.21) into (3.19) gives us

$$|I_1|\le C\int_0^1\frac{(u_x)^2}{u}\mathrm{d}x+\frac{1}{2}\|\tilde{u}_x\|^2. \tag{3.22}$$

The remaining terms are estimated as

- $|I_2|\le C\big(|\beta_1-\beta_2|+|\alpha'|\big)\big(\|\tilde{u}\|^2+1\big)$,
- $|I_5|\le C\big(\varepsilon|\beta_1-\beta_2|+|\beta_1'|+|\beta_2'|\big)\big(\|\tilde{v}\|^2+1\big)$.

Then, we update (3.18) as

$$\begin{aligned}&\frac{1}{2}\frac{\mathrm{d}}{\mathrm{d}t}\left(\|\tilde{u}\|^2+\alpha\|\tilde{v}\|^2+1\right)+\frac{1}{2}\|\tilde{u}_x\|^2+\alpha\varepsilon\|\tilde{v}_x\|^2\\&\le C\left[|\alpha'|+(1+\varepsilon)|\beta_1-\beta_2|+|\beta_1'|+|\beta_2'|\right]\left(\|\tilde{u}\|^2+\alpha\|\tilde{v}\|^2+1\right)+C\int_0^1\frac{(u_x)^2}{u}\mathrm{d}x.\end{aligned} \tag{3.23}$$

Applying Grönwall's inequality to (3.23) and using (3.13) and the assumptions in Theorem 2.1, we obtain

$$\|\tilde{u}(t)\|^2+\alpha(t)\|\tilde{v}(t)\|^2\le C. \tag{3.24}$$

Substituting (3.24) into (3.23), then integrating the resulting inequality with respect to t, we have

$$\int_0^t\|\tilde{u}_x(\tau)\|^2\mathrm{d}\tau\le C, \tag{3.25}$$

where the constant is independent of t. We conclude the proof by noticing $0<\underline{\alpha}\le\alpha(t)$. □

https://doi.org/10.1017/S0956792524000329 Published online by Cambridge University Press

3.3. $L_t^\infty H_x^1$–$L_t^2 H_x^2$–*estimates*

Lemma 3.3. *Under the assumptions of Theorem 2.1, there exists a constant $C > 0$ which is independent of t, such that*

$$\|\tilde{u}_x(t)\|^2 + \|\tilde{v}_x(t)\|^2 + \int_0^t \left(\|\tilde{u}_{xx}(\tau)\|^2 + \varepsilon\|\tilde{v}_{xx}(\tau)\|^2\right) \mathrm{d}\tau \le C.$$

Proof. Taking L^2 inner products of (3.14a) with $-\tilde{u}_{xx}$ and (3.14b) with $-\tilde{v}_{xx}$, respectively, then adding the results, we obtain

$$\begin{aligned}
&\frac{1}{2}\frac{\mathrm{d}}{\mathrm{d}t}\left(\|\tilde{u}_x\|^2 + \|\tilde{v}_x\|^2\right) + \|\tilde{u}_{xx}\|^2 + \varepsilon\|\tilde{v}_{xx}\|^2 \\
&= -\int_0^1 \left[(\tilde{u}\tilde{v})_x + \alpha\tilde{v}_x + (\beta\tilde{u})_x\right] \tilde{u}_{xx}\mathrm{d}x - (\alpha\beta_x - \alpha')\int_0^1 \tilde{u}_{xx}\mathrm{d}x + 2\varepsilon\int_0^1 (\tilde{v}+\beta)\tilde{v}_x\tilde{v}_{xx}\mathrm{d}x \\
&\quad + 2\varepsilon\beta_x\int_0^1 \tilde{v}\tilde{v}_{xx}\mathrm{d}x - \int_0^1 \tilde{u}_x\tilde{v}_{xx}\mathrm{d}x + \int_0^1 (2\varepsilon\beta\beta_x + \beta_t)\tilde{v}_{xx}\mathrm{d}x \equiv \sum_{k=1}^{6} J_k.
\end{aligned} \tag{3.26}$$

Since $\beta = (\beta_2 - \beta_1)x + \beta_1$ and α, β_1, β_2 are uniformly bounded (see Remark 2.2), using the Cauchy–Schwarz, Sobolev and Poincaré inequalities, we can show that

$$\begin{aligned}
|J_1| &\le \frac{1}{4}\|\tilde{u}_{xx}\|^2 + C\left(\|\tilde{v}\|_{L^\infty}^2\|\tilde{u}_x\|^2 + \|\tilde{u}\|_{L^\infty}^2\|\tilde{v}_x\|^2 + \|\tilde{v}_x\|^2 + \|\tilde{u}_x\|^2 + \|\tilde{u}\|^2\right) \\
&\le \frac{1}{4}\|\tilde{u}_{xx}\|^2 + C\left(\|\tilde{u}_x\|^2\|\tilde{v}_x\|^2 + \|\tilde{v}_x\|^2 + \|\tilde{u}_x\|^2\right).
\end{aligned}$$

Since $\alpha'(t)$ is uniformly bounded (see Remark 2.2), we estimate J_2 as

$$|J_2| \le \frac{1}{4}\|\tilde{u}_{xx}\|^2 + C(|\beta_1 - \beta_2|^2 + |\alpha'|^2) \le \frac{1}{4}\|\tilde{u}_{xx}\|^2 + C(|\beta_1 - \beta_2| + |\alpha'|).$$

Similar to the estimate of J_1, we can show that

$$|J_3| \le \frac{\varepsilon}{4}\|\tilde{v}_{xx}\|^2 + C\varepsilon(\|\tilde{v}_x\|^2 + 1)\|\tilde{v}_x\|^2.$$

By the boundedness of the boundary data and Poincaré's inequality, we estimate the remaining terms as:

$$|J_4| + |J_5| + |J_6| \le \frac{\varepsilon}{4}\|\tilde{v}_{xx}\|^2 + C(\varepsilon, \varepsilon^{-1})\big(\|(\tilde{v}_x, \tilde{u}_x)\|^2 + |(\beta_1 - \beta_2, \beta_1', \beta_2')|\big).$$

We remark that the constant $C(\varepsilon, \varepsilon^{-1})$ results from applying the Cauchy–Schwarz inequality to J_5 and J_6 where ε does not appear. Substituting the above estimates into (3.26) gives us

$$\begin{aligned}
&\frac{1}{2}\frac{\mathrm{d}}{\mathrm{d}t}\left(\|\tilde{u}_x\|^2 + \|\tilde{v}_x\|^2\right) + \frac{1}{2}\|\tilde{u}_{xx}\|^2 + \frac{\varepsilon}{2}\|\tilde{v}_{xx}\|^2 \\
&\le C\|\tilde{v}_x\|^2(\|\tilde{u}_x\|^2 + \varepsilon\|\tilde{v}_x\|^2) + C(\varepsilon, \varepsilon^{-1})\big(\|(\tilde{v}_x, \tilde{u}_x)\|^2 + |(\alpha', \beta_1 - \beta_2, \beta_1', \beta_2')|\big).
\end{aligned} \tag{3.27}$$

Applying Grönwall's inequality to (3.27) and using (3.13), (3.25), we obtain

$$\|\tilde{u}_x(t)\|^2 + \|\tilde{v}_x(t)\|^2 + \int_0^t \left(\|\tilde{u}_{xx}(\tau)\|^2 + \varepsilon\|\tilde{v}_{xx}(\tau)\|^2\right) \mathrm{d}\tau \le C(\varepsilon, \varepsilon^{-1}), \tag{3.28}$$

where the constant is independent of t. This completes the proof of Lemma 3.3. □

https://doi.org/10.1017/S0956792524000329 Published online by Cambridge University Press

3.4. $L_t^\infty H_x^2$–$L_t^2 H_x^3$–estimates

Lemma 3.4. *Under the assumptions of Theorem 2.1, there exists a constant $C > 0$ which is independent of t, such that*

$$\|\tilde{u}_{xx}(t)\|^2 + \|\tilde{v}_{xx}(t)\|^2 + \int_0^t \left(\|\tilde{u}_{xxx}(\tau)\|^2 + \varepsilon\|\tilde{v}_{xxx}(\tau)\|^2\right) \mathrm{d}\tau \le C.$$

Proof. Since the information of the higher order spatial derivatives of the solution is unknown at the boundary points, one cannot differentiate the equations with respect to x to estimate the $L_t^\infty H_x^2$ and $L_t^2 H_x^3$ norms of the solution. We turn to the estimation of the temporal derivatives and then utilize the equations to recover the spatial derivatives.

Step 1. Taking ∂_t of (3.14a) and (3.14b), we obtain

$$\tilde{u}_{tt} - (\tilde{u}\tilde{v})_{xt} = \tilde{u}_{xxt} + \alpha'\tilde{v}_x + \alpha\tilde{v}_{xt} + \beta_t\tilde{u}_x + \beta\tilde{u}_{xt} + \beta_{xt}\tilde{u} + \beta_x\tilde{u}_t + \alpha'\beta_x - \alpha\beta_{xt} - \alpha'', \tag{3.29a}$$

$$\begin{aligned}\tilde{v}_{tt} - \tilde{u}_{xt} = {}& \varepsilon\tilde{v}_{xxt} - 2\varepsilon\tilde{v}_t\tilde{v}_x - 2\varepsilon\tilde{v}\tilde{v}_{xt} - 2\varepsilon\beta_t\tilde{v}_x - 2\varepsilon\beta\tilde{v}_{xt} - 2\varepsilon\tilde{v}_t\beta_x - 2\varepsilon\tilde{v}\beta_{xt} - 2\varepsilon\beta_t\beta_x \\ & - 2\varepsilon\beta\beta_{xt} - \beta_{tt}.\end{aligned} \tag{3.29b}$$

Taking L^2 inner product of (3.29a) with $\tilde{u}_t$, we have

$$\begin{aligned}\frac{1}{2}\frac{\mathrm{d}}{\mathrm{d}t}\|\tilde{u}_t\|^2 + \|\tilde{u}_{xt}\|^2 = {}& -\int_0^1 (\tilde{u}\tilde{v})_t\tilde{u}_{xt}\mathrm{d}x + \alpha'\int_0^1 \tilde{v}_x\tilde{u}_t\mathrm{d}x - \alpha\int_0^1 \tilde{v}_t\tilde{u}_{xt}\mathrm{d}x + \int_0^1 \beta_t\tilde{u}_x\tilde{u}_t\mathrm{d}x \\ & + \int_0^1 \beta\tilde{u}_{xt}\tilde{u}_t\mathrm{d}x + \beta_{xt}\int_0^1 \tilde{u}\tilde{u}_t\mathrm{d}x + \beta_x\|\tilde{u}_t\|^2 + (\alpha'\beta_x - \alpha\beta_{xt} - \alpha'')\int_0^1 \tilde{u}_t\mathrm{d}x \equiv \sum_{k=1}^8 K_k.\end{aligned} \tag{3.30}$$

For K_1, we can show that

$$\begin{aligned}|K_1| \le {}& \frac{1}{6}\|\tilde{u}_{xt}\|^2 + 3\left(\|\tilde{u}\|_{L^\infty}^2\|\tilde{v}_t\|^2 + \|\tilde{v}\|_{L^\infty}^2\|\tilde{u}_t\|^2\right) \\ \le {}& \frac{1}{6}\|\tilde{u}_{xt}\|^2 + C\left(\|\tilde{u}\|_{H^1}^2\|\tilde{v}_t\|^2 + \|\tilde{v}\|_{H^1}^2\|\tilde{u}_t\|^2\right) \le \frac{1}{6}\|\tilde{u}_{xt}\|^2 + C\|(\tilde{v}_t, \tilde{u}_t)\|^2,\end{aligned}$$

where we applied Lemmas 3.2 and 3.3. Using the boundedness of the boundary data, we have

$$|K_2| + |K_3| + |K_4| + |K_5| + |K_6| + |K_7| \le \frac{1}{3}\|\tilde{u}_{xt}\|^2 + C\|(\tilde{u}_x, \tilde{v}_x, \tilde{u}_t, \tilde{v}_t)\|^2,$$

where we also invoked Poincaré's inequality. Similarly, K_8 is estimated as

$$\begin{aligned}|K_8| \le {}& |\alpha''|\,\|\tilde{u}_t\|^2 + C\left(|\alpha''| + \|\tilde{u}_t\|^2 + |\alpha'|^2|\beta_1 - \beta_2|^2 + |\alpha|^2(|\beta_1'|^2 + |\beta_2'|^2)\right) \\ \le {}& \frac{1}{2}|\alpha''|\,\|\tilde{u}_t\|^2 + C\left(\|\tilde{u}_t\|^2 + |(\alpha'', \beta_1 - \beta_2, \beta_1', \beta_2')|\right).\end{aligned}$$

Substituting the above estimates into (3.30) gives us

$$\frac{\mathrm{d}}{\mathrm{d}t}\|\tilde{u}_t\|^2 + \|\tilde{u}_{xt}\|^2 \le |\alpha''|\,\|\tilde{u}_t\|^2 + C\left(\|(\tilde{u}_t, \tilde{u}_x, \tilde{v}_t, \tilde{v}_x)\|^2 + |(\alpha'', \beta_1 - \beta_2, \beta_1', \beta_2')|\right). \tag{3.31}$$

Step 2. Taking L^2 inner product of (3.29b) with $\tilde{v}_t$, we obtain

$$\begin{aligned}\frac{1}{2}\frac{\mathrm{d}}{\mathrm{d}t}\|\tilde{v}_t\|^2 + \varepsilon\|\tilde{v}_{xt}\|^2 = {}& -\int_0^1 \tilde{u}_t\tilde{v}_{xt}\mathrm{d}x + 2\varepsilon\int_0^1 \tilde{v}\tilde{v}_t\tilde{v}_{xt}\mathrm{d}x - 2\varepsilon\int_0^1 \beta_t\tilde{v}_x\tilde{v}_t\mathrm{d}x - \varepsilon\beta_x\|\tilde{v}_t\|^2 \\ & - 2\varepsilon\beta_{xt}\int_0^1 \tilde{v}\tilde{v}_t\mathrm{d}x - 2\varepsilon\beta_x\int_0^1 \beta_t\tilde{v}_t\mathrm{d}x - 2\varepsilon\beta_{xt}\int_0^1 \beta\tilde{v}_t\mathrm{d}x - \int_0^1 \beta_{tt}\tilde{v}_t\mathrm{d}x.\end{aligned} \tag{3.32}$$

Using the arguments in **Step 1**, we can show that

$$\frac{\mathrm{d}}{\mathrm{d}t}\|\tilde{v}_t\|^2 + \varepsilon\|\tilde{v}_{xt}\|^2 \le |(\beta_1'', \beta_2'')|\,\|\tilde{v}_t\|^2 + C\left(\|(\tilde{u}_t, \tilde{u}_x, \tilde{v}_t, \tilde{v}_x)\|^2 + |(\beta_1 - \beta_2, \beta_1', \beta_2', \beta_1'', \beta_2'')|\right). \tag{3.33}$$

Note that according to the assumptions of Theorem 2.1 and Lemmas 3.1–3.2, the quantities on the right-hand sides of (3.31) and (3.33), except $\|\tilde{u}_t\|^2$ and $\|\tilde{v}_t\|^2$, are uniformly integrable with respect to t. For

https://doi.org/10.1017/S0956792524000329 Published online by Cambridge University Press

$\|\tilde{u}_t\|^2$ and $\|\tilde{v}_t\|^2$, based on the equations (3.14a) and (3.14b), we can show that

- $\|\tilde{u}_t\|^2 \le C\big(\|(\tilde{u}_x, \tilde{v}_x, \tilde{u}_{xx})\|^2 + |(\alpha', \beta_1 - \beta_2)|\big)$,
- $\|\tilde{v}_t\|^2 \le C\big(\|(\tilde{u}_x, \tilde{v}_x, \tilde{v}_{xx})\|^2 + |(\beta_1 - \beta_2, \beta_1', \beta_2')|\big)$.

Then we update (3.31) and (3.33) as

$$\frac{\mathrm{d}}{\mathrm{d}t}\|\tilde{u}_t\|^2 + \|\tilde{u}_{xt}\|^2 \le |\alpha''|\,\|\tilde{u}_t\|^2 + C\big(\|(\tilde{u}_{xx}, \tilde{u}_x, \tilde{v}_{xx}, \tilde{v}_x)\|^2 + |(\alpha', \alpha'', \beta_1 - \beta_2, \beta_1', \beta_2')|\big),$$

and

$$\frac{\mathrm{d}}{\mathrm{d}t}\|\tilde{v}_t\|^2 + \varepsilon\|\tilde{v}_{xt}\|^2 \le |(\beta_1'', \beta_2'')|\,\|\tilde{v}_t\|^2 + C\big(\|(\tilde{u}_{xx}, \tilde{u}_x, \tilde{v}_{xx}, \tilde{v}_x)\|^2 + |(\alpha', \beta_1 - \beta_2, \beta_1', \beta_2', \beta_1'', \beta_2'')|\big).$$

Applying Grönwall's inequality to the above inequalities, using the assumptions of Theorem 2.1 and Lemmas 3.1–3.3, we can show that

$$\|\tilde{u}_t(t)\|^2 + \|\tilde{v}_t(t)\|^2 + \int_0^t \big(\|\tilde{u}_{xt}(\tau)\|^2 + \varepsilon\|\tilde{v}_{xt}(\tau)\|^2\big)\,\mathrm{d}\tau \le C. \tag{3.34}$$

As a consequence, we can show by using the equations in (3.14) that

$$\|\tilde{u}_{xx}(t)\|^2 + \|\tilde{v}_{xx}(t)\|^2 + \int_0^t \big(\|\tilde{u}_{xxx}(\tau)\|^2 + \varepsilon\|\tilde{v}_{xxx}(\tau)\|^2\big)\,\mathrm{d}\tau \le C.$$

We omit the routine technical details for brevity. This completes the proof of Lemma 3.4. □

Lemma 3.1–Lemma 3.4 established the desired *a priori* estimates of the local solution. The global well-posedness of the IBVP then follows from these estimates and standard continuation argument. To finish the proof of Theorem 2.1, it remains to derive the time decay of the perturbation, which is carried out in the next subsection.

3.5. Decay estimate

Lemma 3.5. *Under the assumptions of Theorem 2.1,* $\|\tilde{u}(t)\|_{H^2} + \|\tilde{v}(t)\|_{H^2} \to 0$, *as* $t \to \infty$.

Proof. Step 1. From Lemma 3.1–Lemma 3.2, we know that $\|\tilde{u}_x(t)\|^2 + \|\tilde{v}_x(t)\|^2 \in L^1(\mathbb{R}_+)$, which, together with Poincaré's inequality, implies $\|\tilde{u}(t)\|^2 + \|\tilde{v}(t)\|^2 \in L^1(\mathbb{R}_+)$. Since $0 < \alpha(t)$ is uniformly bounded, we obtain

$$\|\tilde{u}(t)\|^2 + \alpha(t)\|\tilde{v}(t)\|^2 \in L^1(\mathbb{R}_+). \tag{3.35}$$

Using the assumptions of Theorem 2.1 and Lemma 3.1–Lemma 3.4, we deduce from (3.18) that

$$\Big|\frac{\mathrm{d}}{\mathrm{d}t}\big(\|\tilde{u}\|^2 + \alpha\|\tilde{v}\|^2\big)\Big| \le C\big(\|(\tilde{u}_x, \tilde{v}_x)\|^2 + |(\beta_1 - \beta_2, \alpha', \beta_1', \beta_2')|\big),$$

where the constant is independent of t. Integrating the above inequality gives us

$$\frac{\mathrm{d}}{\mathrm{d}t}\big(\|\tilde{u}(t)\|^2 + \alpha(t)\|\tilde{v}(t)\|^2\big) \in L^1(\mathbb{R}_+). \tag{3.36}$$

From (3.35) and (3.36), $\|\tilde{u}(t)\|^2 + \alpha(t)\|\tilde{v}(t)\|^2 \in W^{1,1}(\mathbb{R}_+)$. Hence, $\|\tilde{u}(t)\|^2 + \alpha(t)\|\tilde{v}(t)\|^2 \to 0$, as $t \to \infty$. Since $0 < \underline{\alpha} \le \alpha(t)$, we conclude $\|\tilde{u}(t)\|^2 + \|\tilde{v}(t)\|^2 \to 0$, as $t \to \infty$.

Step 2. The decay of $\|\tilde{u}_x(t)\|^2 + \|\tilde{v}_x(t)\|^2$ follows by the same idea. Indeed, from (3.26), we have

$$\Big|\frac{\mathrm{d}}{\mathrm{d}t}\big(\|\tilde{u}_x\|^2 + \|\tilde{v}_x\|^2\big)\Big| \le C\big(\|(\tilde{u}_x, \tilde{v}_x, \tilde{u}_{xx}, \tilde{v}_{xx})\|^2 + |(\alpha', \beta_1 - \beta_2, \beta_1', \beta_2')|\big),$$

which, together with the estimates of the solution and the assumptions of Theorem 2.1, implies

$$\frac{\mathrm{d}}{\mathrm{d}t}\big(\|\tilde{u}_x\|^2 + \|\tilde{v}_x\|^2\big) \in L^1(\mathbb{R}_+).$$

https://doi.org/10.1017/S0956792524000329 Published online by Cambridge University Press

Hence, $\|\tilde{u}_x(t)\|^2 + \|\tilde{v}_x(t)\|^2 \in W^{1,1}(\mathbb{R}_+)$, which implies $\|\tilde{u}_x(t)\|^2 + \|\tilde{v}_x(t)\|^2 \to 0$, as $t \to \infty$.

Step 3. For the second order spatial derivatives, we know from (3.34) and Poincaré's inequality that $\|\tilde{u}_t(t)\|^2 + \|\tilde{v}_t(t)\|^2 \in L^1(\mathbb{R}_+)$. By (3.30) and (3.32), we can show that

$$\left|\frac{\mathrm{d}}{\mathrm{d}t}\left(\|\tilde{u}_t\|^2 + \|\tilde{v}_t\|^2\right)\right| \le C\big(\|(\tilde{u}_t, \tilde{v}_t, \tilde{u}_{xt}, \tilde{v}_{xt}, \tilde{u}_x, \tilde{v}_x)\|^2 + |(\alpha', \alpha'', \beta_1 - \beta_2, \beta_1', \beta_2', \beta_1'', \beta_2'')|\big),$$

which, together with the estimates of the solution and the assumptions of Theorem 2.1, implies

$$\frac{\mathrm{d}}{\mathrm{d}t}\left(\|\tilde{u}_t(t)\|^2 + \|\tilde{v}_t(t)\|^2\right) \in L^1(\mathbb{R}_+).$$

Hence, $\|\tilde{u}_t(t)\|^2 + \|\tilde{v}_t(t)\|^2 \in W^{1,1}(\mathbb{R}_+)$, which implies $\|\tilde{u}_t(t)\|^2 + \|\tilde{v}_t(t)\|^2 \to 0$, as $t \to \infty$. According to (3.14), we can show that

$$\|\tilde{u}_{xx}\|^2 + \|\tilde{v}_{xx}\|^2 \le C\big(\|(\tilde{u}_t, \tilde{v}_t, \tilde{u}_x, \tilde{v}_x)\|^2 + |(\alpha', \beta_1 - \beta_2, \beta_1', \beta_2')|\big). \tag{3.37}$$

Since α', $\beta_1 - \beta_2$, β_1' and β_2' belong to $W^{1,1}(\mathbb{R}_+)$, they all tend to zero as $t \to \infty$. Therefore, the decay of $\|\tilde{u}_{xx}(t)\|^2 + \|\tilde{v}_{xx}(t)\|^2$ follows from (3.37) and the decay of the first-order derivatives of the perturbation. This completes the proof of Lemma 3.5. □

4. Proof of Theorem 2.2

This section is devoted to prove Theorem 2.2. Recall system (2.2):

$$u_t - (uv)_x = u_{xx}, \tag{4.1a}$$

$$v_t - u_x = 0, \tag{4.1b}$$

together with the initial and boundary conditions:

$$(u, v)(x, 0) = (u_0, v_0)(x), \quad x \in [0, 1], \tag{4.2a}$$

$$u(0, t) = u(1, t) = \alpha(t), \quad t \ge 0. \tag{4.2b}$$

We stress that some of the *a priori* estimates in the previous section cannot be carried over to (4.1). This can be seen from (3.27), in which the constant blows up when $\varepsilon \to 0$. We adapt a different approach to estimate higher order spatial derivatives of the solution.

Step 1. First we note that (3.4) is still valid when $\varepsilon = 0$. We record it here for convenience:

$$\frac{\mathrm{d}}{\mathrm{d}t}E(u, \alpha) + \int_0^1 \frac{(u_x)^2}{u}\mathrm{d}x = -\int_0^1 v u_x \mathrm{d}x - \int_0^1 (u - \alpha)\frac{\alpha'}{\alpha}\mathrm{d}x, \tag{4.3}$$

where $E(u, \alpha)$ is the same as before. Integrating (4.1b) with respect to x and t and using the boundary conditions for u, we have

$$\int_0^1 v(x, t)\mathrm{d}x = \int_0^1 v(x, 0)\mathrm{d}x \equiv \overline{v}. \tag{4.4}$$

Since $\overline{v}$ is a constant, we easily obtain

$$(v - \overline{v})_t - u_x = 0. \tag{4.5}$$

Taking L^2 inner product of (4.5) with $(v - \overline{v})$, we obtain

$$\frac{1}{2}\frac{\mathrm{d}}{\mathrm{d}t}\|v - \overline{v}\|^2 = \int_0^1 u_x(v - \overline{v})\mathrm{d}x = \int_0^1 u_x v \mathrm{d}x, \tag{4.6}$$

where the integral of $u_x\overline{v}$ is zero, since $\overline{v}$ is a constant and the boundary values of u match at the endpoints. Taking the sum of (4.3) and (4.6) gives us

$$\frac{\mathrm{d}}{\mathrm{d}t}\left(E(u, \alpha) + \frac{1}{2}\|v - \overline{v}\|^2\right) + \int_0^1 \frac{(u_x)^2}{u}\mathrm{d}x = -\int_0^1 (u - \alpha)\frac{\alpha'}{\alpha}\mathrm{d}x. \tag{4.7}$$

https://doi.org/10.1017/S0956792524000329 Published online by Cambridge University Press

Similar to **Step 2** of the proof of Lemma 3.1, we can show that

$$\frac{\mathrm{d}}{\mathrm{d}t}\Big(E(u,\alpha)+\frac{1}{2}\|v-\overline{v}\|^2\Big)+\int_0^1\frac{(u_x)^2}{u}\mathrm{d}x\le\frac{|\alpha'|}{\underline{\alpha}}E(u,\alpha)+e|\alpha'|. \tag{4.8}$$

Applying Grönwall's inequality and using the assumptions for α, we obtain

$$E(u,\alpha)(t)+\|(v-\overline{v})(t)\|^2+\int_0^t\int_0^1\frac{(u_x)^2}{u}\mathrm{d}x\mathrm{d}\tau\le C, \tag{4.9}$$

where the constant on the right-hand side is independent of t.

Step 2. Again, we define the perturbed variables: $\tilde{u}(x,t)=u(x,t)-\alpha(t)$, $\tilde{v}(x,t)=v(x,t)-\overline{v}$. Similar to (3.14), we have

$$\tilde{u}_t-(\tilde{u}\tilde{v})_x=\tilde{u}_{xx}+\alpha\tilde{v}_x+\overline{v}\tilde{u}_x-\alpha', \tag{4.10a}$$

$$\tilde{v}_t-\tilde{u}_x=0. \tag{4.10b}$$

Taking L^2 inner product of (4.10a) with $\tilde{u}$, we have

$$\frac{1}{2}\frac{\mathrm{d}}{\mathrm{d}t}\|\tilde{u}\|^2+\|\tilde{u}_x\|^2=-\int_0^1\tilde{u}\tilde{v}\tilde{u}_x\mathrm{d}x+\alpha\int_0^1\tilde{v}_x\tilde{u}\mathrm{d}x-\alpha'\int_0^1\tilde{u}\mathrm{d}x. \tag{4.11}$$

Taking L^2 inner product of (4.10b) with $\alpha\tilde{v}$, we obtain

$$\frac{1}{2}\frac{\mathrm{d}}{\mathrm{d}t}\big(\alpha\|\tilde{v}\|^2\big)=\alpha\int_0^1\tilde{u}_x\tilde{v}\mathrm{d}x+\frac{\alpha'}{2}\|\tilde{v}\|^2. \tag{4.12}$$

Taking the sum of (4.11) and (4.12) gives us

$$\frac{1}{2}\frac{\mathrm{d}}{\mathrm{d}t}\big(\|\tilde{u}\|^2+\alpha\|\tilde{v}\|^2\big)+\|\tilde{u}_x\|^2=-\int_0^1\tilde{u}\tilde{v}\tilde{u}_x\mathrm{d}x-\alpha'\int_0^1\tilde{u}\mathrm{d}x+\frac{\alpha'}{2}\|\tilde{v}\|^2. \tag{4.13}$$

The estimate of the first integral on the right-hand side of (4.13) is identical to (3.23), which is recorded here for convenience:

$$\int_0^1\tilde{u}\tilde{v}\tilde{u}_x\mathrm{d}x\le C\int_0^1\frac{(u_x)^2}{u}\mathrm{d}x+\frac{1}{2}\|\tilde{u}_x\|^2. \tag{4.14}$$

The second integral on the right-hand side of (4.13) is estimated as

$$\alpha'\int_0^1\tilde{u}\mathrm{d}x\le|\alpha'|\,\|\tilde{u}\|\le\frac{|\alpha'|}{2}\|\tilde{u}\|^2+\frac{|\alpha'|}{2}. \tag{4.15}$$

Substituting (4.14) and (4.15) into (4.13), we obtain

$$\frac{\mathrm{d}}{\mathrm{d}t}\big(\|\tilde{u}\|^2+\alpha\|\tilde{v}\|^2\big)+\|\tilde{u}_x\|^2\le C|\alpha'|\big(\|\tilde{u}\|^2+\alpha\|\tilde{v}\|^2\big)+C\Big(\int_0^1\frac{(u_x)^2}{u}\mathrm{d}x+|\alpha'|\Big), \tag{4.16}$$

where we utilised the strictly positive lower bound of α for the third term on the right-hand side of (4.13). Applying Grönwall's inequality and using the assumptions for α, we can show that

$$\|\tilde{u}(t)\|^2+\|\tilde{v}(t)\|^2+\int_0^t\|\tilde{u}_x(\tau)\|^2\mathrm{d}\tau\le C, \tag{4.17}$$

where (4.9) is applied and the constant C is independent of t.

Step 3. This step is the major difference between the proof of Theorems 2.1 and 2.2. The following equation, obtained by substituting $\tilde{u}_{xx}=\tilde{v}_{xt}$ into (4.10a),

$$\tilde{v}_{xt}+\alpha\tilde{v}_x=\tilde{u}_t-(\tilde{u}\tilde{v})_x-\overline{v}\tilde{u}_x+\alpha', \tag{4.18}$$

serves as the ground for the time integrability of $\tilde{v}_x$. Taking L^2 inner product of (4.18) with $\tilde{v}_x$, we have

$$\frac{1}{2}\frac{\mathrm{d}}{\mathrm{d}t}\|\tilde{v}_x\|^2+\alpha\|\tilde{v}_x\|^2=\int_0^1\tilde{u}_t\tilde{v}_x\mathrm{d}x-\int_0^1(\tilde{u}\tilde{v})_x\tilde{v}_x\mathrm{d}x-\overline{v}\int_0^1\tilde{u}_x\tilde{v}_x\mathrm{d}x+\alpha'\int_0^1\tilde{v}_x\mathrm{d}x. \tag{4.19}$$

https://doi.org/10.1017/S0956792524000329 Published online by Cambridge University Press

Using (4.10b), we rewrite the first integral on the right-hand side of (4.19) as

$$\int_0^1 \tilde{u}_t\tilde{v}_x\mathrm{d}x = \frac{\mathrm{d}}{\mathrm{d}t}\int_0^1 \tilde{u}\tilde{v}_x\mathrm{d}x - \int_0^1 \tilde{u}\tilde{v}_{xt}\mathrm{d}x = \frac{\mathrm{d}}{\mathrm{d}t}\int_0^1 \tilde{u}\tilde{v}_x\mathrm{d}x + \|\tilde{u}_x\|^2. \tag{4.20}$$

Substituting (4.20) into (4.19), we obtain

$$\frac{\mathrm{d}}{\mathrm{d}t}\Big(\frac{1}{2}\|\tilde{v}_x\|^2 - \int_0^1 \tilde{u}\tilde{v}_x\mathrm{d}x\Big) + \alpha\|\tilde{v}_x\|^2 = \|\tilde{u}_x\|^2 - \int_0^1 \left[(\tilde{u}\tilde{v})_x + \overline{v}\tilde{u}_x - \alpha'\right]\tilde{v}_x\mathrm{d}x. \tag{4.21}$$

The three pieces in the integral on the right-hand side of (4.21) are estimated as

- $\displaystyle\int_0^1 (\tilde{u}\tilde{v})_x\tilde{v}_x\mathrm{d}x \le C\|\tilde{u}_x\|\|\tilde{v}_x\|\|\tilde{v}_x\| \le \frac{\alpha}{6}\|\tilde{v}_x\|^2 + \frac{C}{\alpha}\|\tilde{u}_x\|^2\|\tilde{v}_x\|^2,$
- $\displaystyle\overline{v}\int_0^1 \tilde{u}_x\tilde{v}_x\mathrm{d}x \le C\|\tilde{u}_x\|\|\tilde{v}_x\| \le \frac{\alpha}{6}\|\tilde{v}_x\|^2 + \frac{C}{\alpha}\|\tilde{u}_x\|^2,$
- $\displaystyle\alpha'\int_0^1 \tilde{v}_x\mathrm{d}x \le |\alpha'|\|\tilde{v}_x\| \le \frac{\alpha}{6}\|\tilde{v}_x\|^2 + \frac{C}{\alpha}|\alpha'|^2.$

Substituting these estimates into (4.21) gives us

$$\frac{\mathrm{d}}{\mathrm{d}t}\Big(\frac{1}{2}\|\tilde{v}_x\|^2 - \int_0^1 \tilde{u}\tilde{v}_x\mathrm{d}x\Big) + \frac{\alpha}{2}\|\tilde{v}_x\|^2 \le C\|\tilde{u}_x\|^2\|\tilde{v}_x\|^2 + C\big(\|\tilde{u}_x\|^2 + |\alpha'|\big), \tag{4.22}$$

where we used the information that $\alpha(t) \ge \underline{\alpha} > 0$ and that $|\alpha'|$ is uniformly bounded. According to (4.17), there is a constant, denoted by $\overline{U}_1$, such that $\|\tilde{u}\|^2 \le \overline{U}_1$. Since

$$\Big|\int_0^1 \tilde{u}\tilde{v}_x\mathrm{d}x\Big| \le \|\tilde{u}\|^2 + \frac{1}{4}\|\tilde{v}_x\|^2 \le \overline{U}_1 + \frac{1}{4}\|\tilde{v}_x\|^2,$$

we know that

$$E_1(t) := \frac{1}{2}\|\tilde{v}_x\|^2 - \int_0^1 \tilde{u}\tilde{v}_x\mathrm{d}x + \overline{U}_1 \ge \frac{1}{4}\|\tilde{v}_x\|^2. \tag{4.23}$$

Then we update (4.22) as

$$\frac{\mathrm{d}}{\mathrm{d}t}E_1(t) + \frac{\alpha}{2}\|\tilde{v}_x\|^2 \le C\|\tilde{u}_x\|^2E_1(t) + C\big(\|\tilde{u}_x\|^2 + |\alpha'|\big). \tag{4.24}$$

Applying Grönwall's inequality, using (4.17) and the assumptions for α, we can show that

$$\|\tilde{v}_x(t)\|^2 + \int_0^t \|\tilde{v}_x(\tau)\|^2\mathrm{d}\tau \le C, \tag{4.25}$$

where (4.23) is applied and the constant on the right-hand side is independent of t.

Step 4. Taking L^2 inner product of (4.10a) with $-\tilde{u}_{xx}$, we have

$$\frac{1}{2}\frac{\mathrm{d}}{\mathrm{d}t}\|\tilde{u}_x\|^2 + \|\tilde{u}_{xx}\|^2 = -\int_0^1 \left[(\tilde{u}\tilde{v})_x + \alpha\tilde{v}_x + \overline{v}\tilde{u}_x - \alpha'\right]\tilde{u}_{xx}\mathrm{d}x. \tag{4.26}$$

The integral on the right-hand side of (4.26) is estimated as

$$\int_0^1 \left[(\tilde{u}\tilde{v})_x + \alpha\tilde{v}_x + \overline{v}\tilde{u}_x - \alpha'\right]\tilde{u}_{xx}\mathrm{d}x \le C\big(\|\tilde{u}_x\|\|\tilde{v}_x\| + \|\tilde{v}_x\| + \|\tilde{u}_x\| + |\alpha'|\big)\|\tilde{u}_{xx}\|.$$

Substituting the above into (4.26) and applying the Cauchy–Schwarz inequality, we obtain

$$\frac{\mathrm{d}}{\mathrm{d}t}\|\tilde{u}_x\|^2 + \|\tilde{u}_{xx}\|^2 \le C\|\tilde{u}_x\|^2\|\tilde{v}_x\|^2 + C\big(\|\tilde{u}_x\|^2 + \|\tilde{v}_x\|^2 + |\alpha'|\big), \tag{4.27}$$

where the uniform boundedness of $|\alpha'|$ is used. Applying Grönwall's inequality to (4.27), using (4.17), (4.25) and the assumptions for α, we can show that

https://doi.org/10.1017/S0956792524000329 Published online by Cambridge University Press

$$\|\tilde{u}_x(t)\|^2 + \int_0^t \|\tilde{u}_{xx}(\tau)\|^2 \mathrm{d}\tau \leq C, \tag{4.28}$$

where the constant on the right-hand side is independent of t.

Step 5. Differentiating (4.10a) with respect to t, we have

$$\tilde{u}_{tt} - (\tilde{u}\tilde{v})_{xt} = \tilde{u}_{xxt} + (\alpha\tilde{v})_{xt} + \bar{v}\tilde{u}_{xt} - \alpha''. \tag{4.29}$$

Taking L^2 inner product of (4.29) with $\tilde{u}_t$ and integrating by parts, we obtain

$$\frac{1}{2}\frac{\mathrm{d}}{\mathrm{d}t}\|\tilde{u}_t\|^2 + \|\tilde{u}_{xt}\|^2 = -\int_0^1 (\tilde{u}\tilde{v})_t\tilde{u}_{xt}\mathrm{d}x - \int_0^1 (\alpha\tilde{v})_t\tilde{u}_{xt}\mathrm{d}x - \alpha''\int_0^1 \tilde{u}_t\mathrm{d}x. \tag{4.30}$$

The integrals on the right-hand side of (4.30) are estimated as

- $\displaystyle\int_0^1 (\tilde{u}\tilde{v})_t\tilde{u}_{xt}\mathrm{d}x \leq C\big(\|\tilde{u}_x\|\|\tilde{v}_t\| + \|\tilde{v}_x\|\|\tilde{u}_t\|\big)\|\tilde{u}_{xt}\|,$
- $\displaystyle\int_0^1 (\alpha\tilde{v})_t\tilde{u}_{xt}\mathrm{d}x \leq \big(|\alpha'|\|\tilde{v}\| + |\alpha|\|\tilde{v}_t\|\big)\|\tilde{u}_{xt}\|,$
- $\displaystyle\alpha''\int_0^1 \tilde{u}_t\mathrm{d}x \leq \frac{|\alpha''|}{2} + \frac{|\alpha''|}{2}\|\tilde{u}_t\|^2.$

Using these estimates and the Cauchy-Schwarz inequality, we update (4.30) as

$$\begin{aligned}\frac{\mathrm{d}}{\mathrm{d}t}\|\tilde{u}_t\|^2 + \|\tilde{u}_{xt}\|^2 &\leq C\big(\|\tilde{v}_x\|^2 + |\alpha''|\big)\|\tilde{u}_t\|^2 + C\big(\|\tilde{u}_x\|^2\|\tilde{v}_t\|^2 + \|\tilde{v}\|^2 + \|\tilde{v}_t\|^2 + |\alpha''|\big)\\ &\leq C\big(\|\tilde{v}_x\|^2 + |\alpha''|\big)\|\tilde{u}_t\|^2 + C\big(\|\tilde{u}_x\|^2 + \|\tilde{v}_x\|^2 + |\alpha''|\big),\end{aligned} \tag{4.31}$$

where we replaced $\tilde{v}_t$ by $\tilde{u}_x$ and utilised (4.28) and the uniform boundedness of $|\alpha'|$ and $|\alpha|$, together with Poincaré's inequality for $\tilde{v}$ (since it is mean free). Applying Grönwall's inequality gives us

$$\|\tilde{u}_t(t)\|^2 + \int_0^t \|\tilde{u}_{xt}(\tau)\|^2\mathrm{d}\tau \leq C. \tag{4.32}$$

As a consequence of (4.32), (4.10a) and previous estimates, we have

$$\|\tilde{u}_{xx}(t)\|^2 \leq C\big(\|\tilde{u}_t\|^2 + \|\tilde{u}_x\|^2\|\tilde{v}_x\|^2 + \|\tilde{v}_x\|^2 + \|\tilde{u}_x\|^2 + |\alpha'|^2\big) \leq C, \tag{4.33}$$

where the constant C is independent of t.

Step 6. Taking ∂_x of (4.18) gives us

$$\tilde{v}_{xxt} + \alpha\tilde{v}_{xx} = \tilde{u}_{xt} - (\tilde{u}\tilde{v})_{xx} - \bar{v}\tilde{u}_{xx}. \tag{4.34}$$

Taking L^2 inner product of (4.34) with $\tilde{v}_{xx}$, we have

$$\frac{1}{2}\frac{\mathrm{d}}{\mathrm{d}t}\|\tilde{v}_{xx}\|^2 + \alpha\|\tilde{v}_{xx}\| = \int_0^1 \tilde{u}_{xt}\tilde{v}_{xx}\mathrm{d}x - \int_0^1 (\tilde{u}\tilde{v})_{xx}\tilde{v}_{xx}\mathrm{d}x - \bar{v}\int_0^1 \tilde{u}_{xx}\tilde{v}_{xx}\mathrm{d}x. \tag{4.35}$$

The integrals on the right-hand side are estimated as:

- $\displaystyle\int_0^1 \tilde{u}_{xt}\tilde{v}_{xx}\mathrm{d}x \leq C\|\tilde{u}_{xt}\|^2 + \frac{\alpha}{6}\|\tilde{v}_{xx}\|^2,$
- $\displaystyle\int_0^1 (\tilde{u}\tilde{v})_{xx}\tilde{v}_{xx}\mathrm{d}x \leq C\big(\|\tilde{v}_x\|^2\|\tilde{u}_{xx}\|^2 + \|\tilde{u}_x\|^2\|\tilde{v}_{xx}\|^2\big) + \frac{\alpha}{6}\|\tilde{v}_{xx}\|^2,$
- $\displaystyle\bar{v}\int_0^1 \tilde{u}_{xx}\tilde{v}_{xx}\mathrm{d}x \leq C\|\tilde{u}_{xx}\|^2 + \frac{\alpha}{6}\|\tilde{v}_{xx}\|^2.$

Then we update (4.35) as

$$\frac{1}{2}\frac{\mathrm{d}}{\mathrm{d}t}\|\tilde{v}_{xx}\|^2 + \frac{\alpha}{2}\|\tilde{v}_{xx}\| \leq C\|\tilde{u}_x\|^2\|\tilde{v}_{xx}\|^2 + C\big(\|\tilde{u}_{xt}\|^2 + \|\tilde{u}_{xx}\|^2\big), \tag{4.36}$$

https://doi.org/10.1017/S0956792524000329 Published online by Cambridge University Press

where we used (4.25) for the estimate of $\|\tilde{v}_x(t)\|$. Applying Grönwall's inequality, we obtain

$$\|\tilde{v}_{xx}(t)\|^2 + \int_0^t \|\tilde{v}_{xx}(\tau)\|^2 \mathrm{d}\tau \leq C. \tag{4.37}$$

As a consequence of (4.37), (4.10a) and previous estimates, we can show that

$$\int_0^t \|\tilde{u}_{xxx}(\tau)\|^2 \mathrm{d}\tau \leq C, \tag{4.38}$$

where the constant on the right-hand side is independent of t. The routine technical details are omitted for brevity. This completes the proof of the *a priori* estimates of the solution, as stated in Theorem 2.2. Moreover, the time decay of the perturbation follows from the same spirit in the previous section. The proof of Theorem 2.2 is thus complete.

5. Numerical studies

In this section, we carry out numerical tests to study the dynamical properties of solutions to (2.1), and those of (2.2). In particular, we 1) provide numerical confirmation of the rigorous qualitative results established in Theorems 2.1-2.2, 2) explore the steady states of the solutions when relaxing some of the assumptions in the theorems and 3) determine whether the solutions converge to time-periodic states when the boundary data are periodic in time.

In order to study the dynamical behavior of the solutions subject to time-periodic boundary conditions, we introduce the following definition.

Definition 5.1. *We say that a function $g(x,t)$ defined in $\Omega \times [0,\infty)$ converges to a time-periodic state if there exists $T > 0$ such that for any $\epsilon > 0$, there exists $t^* > 0$, such that*

$$|g(x,t+T) - g(x,t)| \leq \epsilon$$

for any $(x,t) \in \Omega \times [t^*, \infty)$

For the simulations in this section, we make use of an explicit finite-difference scheme to solve (2.1) and (2.2) with a second-order approximation of spatial derivatives with a temporal mesh, $\Delta t = \frac{(\Delta x)^2}{2}$, and a spatial mesh, $\Delta x < \sqrt{\frac{\varepsilon}{10}}$, similar to what would be chosen for the heat equation in order to avoid that the numerical diffusion dominates the chemical diffusion. The domain for the system is the unit interval $[0,1]$ with time-dependent boundary data α_1, α_2 and β_1, β_2. For the following results, we have used initial data $u(x,0) = 0.3 + 0.1\sin^2(2\pi x)$ and $v(x,0) = 0.2\sin^2(2\pi x)$. We would like to point out that the large–time behaviors of the solutions do not vary for similar kinds of initial data. For consistency, we use the same initial conditions and $N = 200$ throughout the computations in this section.

We define $A(x,t) = (\alpha_2 - \alpha_1)x + \alpha_1$ and $B(x,t) = (\beta_2 - \beta_1)x + \beta_1$, the linear interpolation of the boundary data, $\tilde{u} = u - A$ and $\tilde{v} = v - B$. Moreover, throughout this section, the letters with overhead bar denote real constants.

5.1. Solutions of (2.1) with converging boundary data

We study the existence of steady states of solutions to (2.1) with different converging conditions on the boundary data. For these computations, we use $\varepsilon = 0.7$.

Case 1: $\boxed{\alpha_1 = \alpha_2 \to \bar{\alpha},\ \ \beta_1 \neq \beta_2,\ \ \beta_1 \to \bar{\beta} \leftarrow \beta_2}$

The solution (u,v) converges to the steady state $(\bar{\alpha}, \bar{\beta})$ as proved in Theorem 2.1.

In this case, we plot u, v, A, B with $\alpha_1 = 0.7 + \exp(-200000t) = \alpha_2$, $\beta_1 = 0.3 + 1/(1 + 10000t)$ and $\beta_2 = 0.3 + 1/(4 + 1000t)$. Figure 1a plots the solution (u,v) and the linear interpolation (A,B) at time $t = 0.168$, with $\alpha_1 = 0.7 = \alpha_2$, $\beta_1 = 0.301$, $\beta_2 = 0.306$. Figure 1b plots (u,v,A,B) at time $t = 49.9$, with

https://doi.org/10.1017/S0956792524000329 Published online by Cambridge University Press

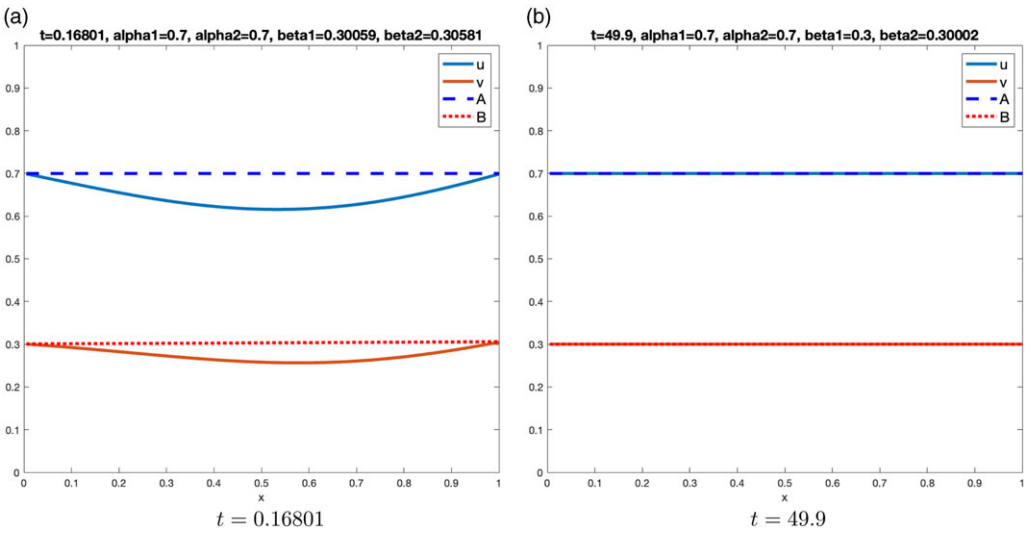

Figure 1. *Solution of (2.1) with* $\alpha_1 = \alpha_2 \to \bar{\alpha}$, $\beta_1 \neq \beta_2$, $\beta_1 \to \bar{\beta} \leftarrow \beta_2$.

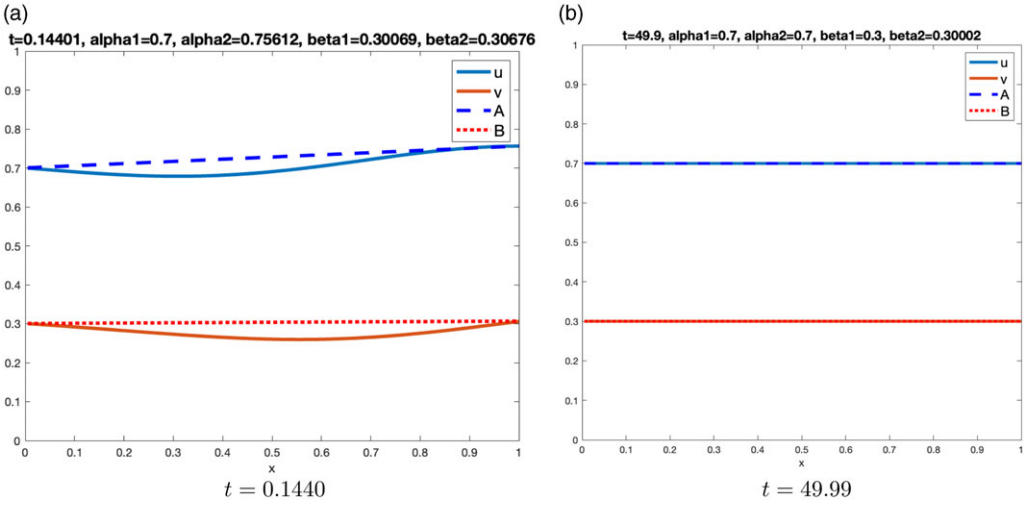

Figure 2. *Solution of (2.1) with* $\alpha_1 \neq \alpha_2$, $\alpha_1 \to \bar{\alpha} \leftarrow \alpha_2$, $\beta_1 \neq \beta_2$, $\beta_1 \to \bar{\beta} \leftarrow \beta_2$.

$\alpha_1 = 0.7 = \alpha_2$, $\beta_1 = 0.3002$, $\beta_2 = 0.3018$. In particular, we observe that the solution reaches the steady state $(\bar{\alpha}, \bar{\beta}) = (0.7, 0.3)$, as $t \to \infty$.

Case 2: $\boxed{\alpha_1 \neq \alpha_2,\ \alpha_1 \to \bar{\alpha} \leftarrow \alpha_2,\ \beta_1 \neq \beta_2,\ \beta_1 \to \bar{\beta} \leftarrow \beta_2}$

The solution (u, v) converges to the steady state $(\bar{\alpha}, \bar{\beta})$.

In this case, we plot u, v, A, B with $\alpha_1 = 0.7 + \exp(-200000t)$, $\alpha_2 = 0.7 + \exp(-20t)$, $\beta_1 = 0.3 + 1/(1 + 10000t)$ and $\beta_2 = 0.3 + 1/(4 + 1000t)$. Figure 2a plots the solution (u, v) and the linear interpolation (A, B) at time $t = 0.1440$, with $\alpha_1 = 0.7$, $\alpha_2 = 0.756$, $\beta_1 = 0.300$, $\beta_2 = 0.306$. Figure 2b plots (u, v, A, B) at time $t = 49.99$, with $\alpha_1 = 0.7 = \alpha_2$, $\beta_1 = 0.3$, $\beta_2 = 0.3002$. In particular, we observe that the solution reaches the steady state $(\bar{\alpha}, \bar{\beta}) = (0.7, 0.3)$ as in Case 1.

https://doi.org/10.1017/S0956792524000329 Published online by Cambridge University Press

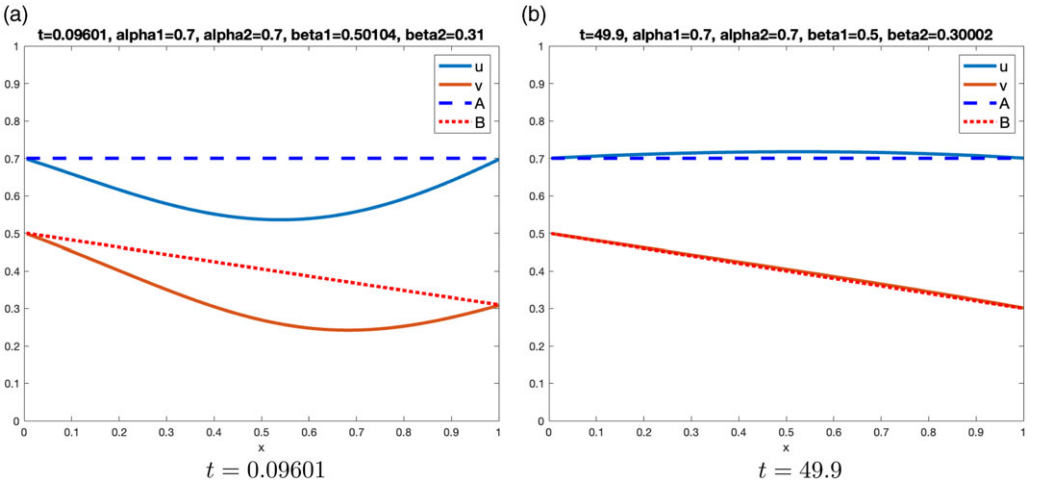

Figure 3. *Solution of (2.1) with* $\alpha_1 = \alpha_2 \to \bar{\alpha}$, $\beta_1 \to \bar{\beta}_1 \neq \bar{\beta}_2 \leftarrow \beta_2$..

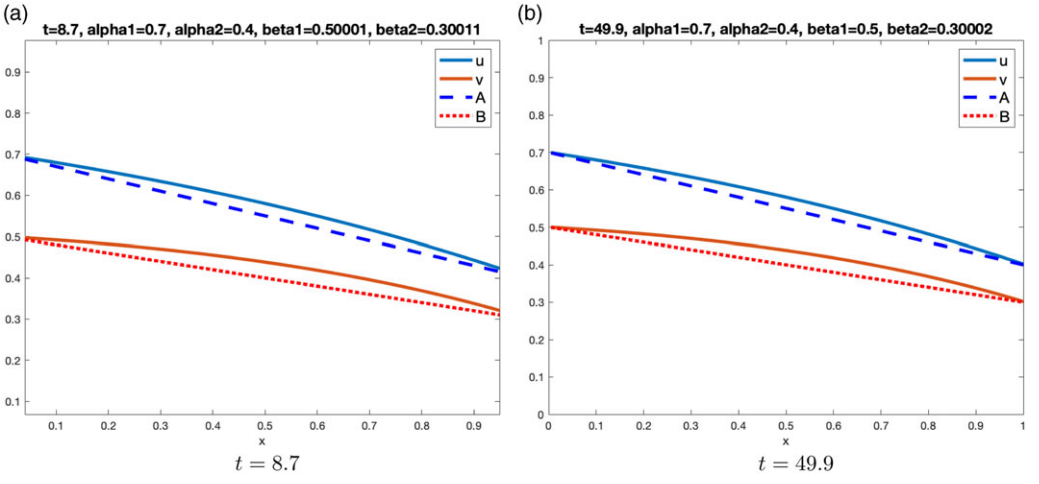

Figure 4. *Solution of (2.1) with* $\alpha_1 \to \bar{\alpha}_1 \neq \bar{\alpha}_2 \leftarrow \alpha_2$, $\beta_1 \to \bar{\beta}_1 \neq \bar{\beta}_2 \leftarrow \beta_2$.

Case 3: $\boxed{\alpha_1 = \alpha_2 \to \bar{\alpha},\ \ \beta_1 \to \bar{\beta}_1 \neq \bar{\beta}_2 \leftarrow \beta_2}$

The solution (u, v) has a steady state different from $\big(\bar{\alpha}, (\bar{\beta}_2 - \bar{\beta}_1)x + \bar{\beta}_1\big)$.

In this case, we plot u, v, A, B with $\alpha_1 = 0.7 + \exp(-200000t) = \alpha_2$, $\beta_1 = 0.5 + 1/(1 + 10000t)$ and $\beta_2 = 0.3 + 1/(4 + 1000t)$. Figure 3a plots the solution (u, v) and the linear interpolation (A, B) at time $t = 0.168$, with $\alpha_1 = 0.7 = \alpha_2$, $\beta_1 = 0.301$, $\beta_2 = 0.306$. Figure 3b shows (u, v, A, B) at time $t = 49.9$, with $\alpha_1 = 0.7 = \alpha_2$, $\beta_1 = 0.500$, $\beta_2 = 0.300$. In particular, we observe that the solution reaches a steady state different from $\big(\bar{\alpha}, (\bar{\beta}_2 - \bar{\beta}_1)x + \bar{\beta}_1\big) = \big(0.7, -0.2x + 0.5\big)$.

Case 4: $\boxed{\alpha_1 \to \bar{\alpha}_1 \neq \bar{\alpha}_2 \leftarrow \alpha_2,\ \ \beta_1 \to \bar{\beta}_1 \neq \bar{\beta}_2 \leftarrow \beta_2}$

The solution (u, v) has a steady state different from $\big((\bar{\alpha}_2 - \bar{\alpha}_1)x + \bar{\alpha}_1, (\bar{\beta}_2 - \bar{\beta}_1)x + \bar{\beta}_1\big)$.

In this case, we plot u, v, A, B with $\alpha_1 = 0.7 + \exp(-200000t)$, $\alpha_2 = 0.4 + \exp(-200000t)$, $\beta_1 = 0.5 + 1/(1 + 10000t)$ and $\beta_2 = 0.3 + 1/(4 + 1000t)$. Figure 4a plots the solution (u, v) and the linear interpolation (A, B) at time $t = 8.7$, with $\alpha_1 = 0.7, \alpha_2 = 0.4$, $\beta_1 = 0.500, \beta_2 = 0.300$. Figure 4b plots

https://doi.org/10.1017/S0956792524000329 Published online by Cambridge University Press

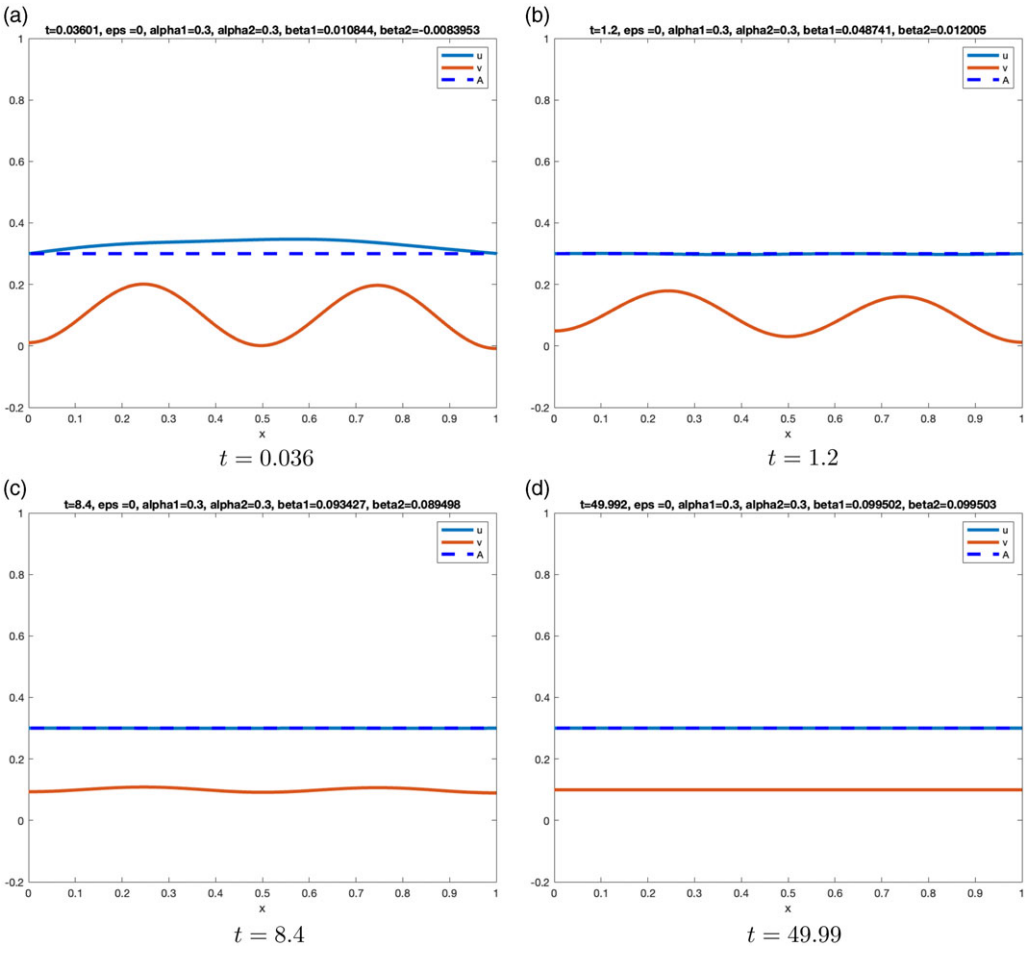

Figure 5. *Solution of (2.2) with* $\alpha_1 = \alpha_2 \to \bar{\alpha}$.

(u, v, A, B) at time $t = 49.9$, with $\alpha_1 = 0.7, \alpha_2 = 0.4$, $\beta_1 = 0.500, \beta_2 = 0.300$. In particular, we observe that the solution reaches a steady state different from $\big((\bar{\alpha}_2 - \bar{\alpha}_1)x + \bar{\alpha}_1, (\bar{\beta}_2 - \bar{\beta}_1)x + \bar{\beta}_1\big) = \big(-0.3x + 0.7, -0.2x + 0.5\big)$.

5.2 Solutions of (2.2) with converging boundary data

This section contains numerical studies of steady state solutions of (2.2) with different converging boundary conditions. For simulations in this section, we use the boundary data α_1, α_2 for u, but notice that the boundary conditions for v cannot be imposed. In this case, they are implicit by (2.2b). Numerically, this presents a challenge that we have overcome by computing explicitly the values at the boundary at each step using (2.2b). Throughout these computations $\varepsilon = 0$, we observe the following.

Case 1: $\boxed{\alpha_1 = \alpha_2 \to \bar{\alpha}}$

The solution (u, v) converges to the steady state $(\bar{\alpha}, \bar{v})$ as proved in Theorem 2.2.

In this case, we plot u, v, A with $\alpha_1 = 0.3 + \exp(-200000t) = \alpha_2$. Notice that the average of v_0, $\bar{v} = 0.1$. Figure 5 shows the evolution in time of the solution (u, v) and the linear interpolation A at times $t = 0.036$, $t = 1.2$, $t = 8.4$ and $t = 49.99$. In particular, we observe that the solution approaches the steady

https://doi.org/10.1017/S0956792524000329 Published online by Cambridge University Press

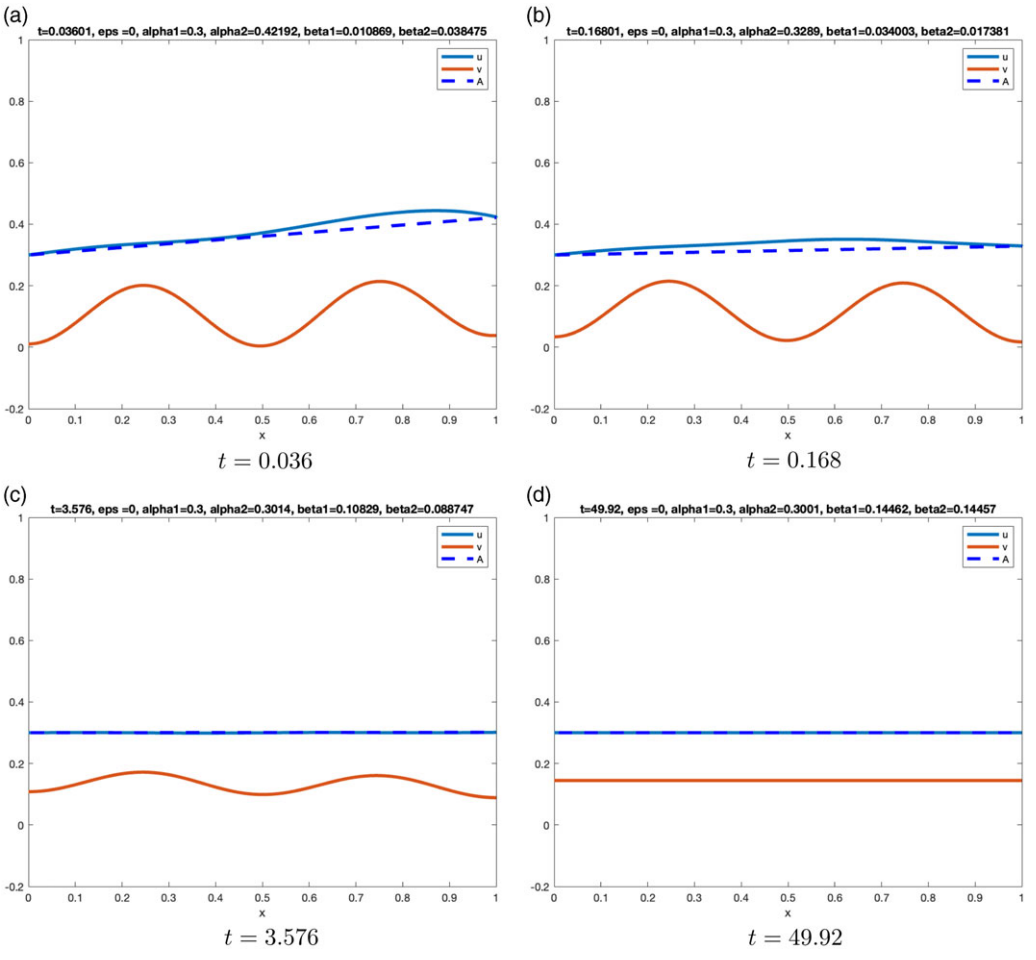

Figure 6. *Solution of (2.2) with* $\alpha_1 \neq \alpha_2$, $\alpha_1 \to \bar{\alpha} \leftarrow \alpha_2$.

state $(A, \bar{v}) = (0.3, 0.1)$, as $t \to \infty$. Notice that even if the chemical diffusion coefficient is zero, the function v still smooths up and converges to its initial average, as predicted in Theorem 2.2.

Case 2: $\boxed{\alpha_1 \neq \alpha_2, \ \alpha_1 \to \bar{\alpha} \leftarrow \alpha_2}$

In this case, u converges to $\bar{\alpha}$ and v converges to a steady–state different from $\bar{v}$.

We plot u, v, A with $\alpha_1 = 0.3 - \exp(-200000t)$ and $\alpha_2 = 0.3 + 1/(1 + 200t)$. Figure 6 shows the evolution in time of the solution (u, v) at times $t = 0.036$, $t = 0.168$, $t = 3.576$, and $t = 49.92$. In particular, we observe that u converges to the steady state $\bar{\alpha} = 0.3$, but v converges to a steady–state different from $\bar{v} = 0.1$. This shows that the assumptions in Theorem 2.2 are in fact necessary.

Case 3: $\boxed{\alpha_1 \to \bar{\alpha}_1 \neq \bar{\alpha}_2 \leftarrow \alpha_2}$

The solution u converges to a steady state different from $(\bar{\alpha}_2 - \bar{\alpha}_1)x + \bar{\alpha}_1$, but v keeps growing or decaying depending on $\alpha_2 - \alpha_1$ being negative or positive respectively.

In this case, we plot u, v, A with $\alpha_1 = 0.7 + \exp(-200000t)$ and $\alpha_2 = 0.3 + \exp(-200000t)$. Figure 7 shows the evolution in time of the solution (u, v) at times $t = 0.072$, $t = 0.372$, $t = 0.612$ and $t = 49.99$. In particular, we observe that u reaches a steady state different from $(\bar{\alpha}_2 - \bar{\alpha}_1)x + \bar{\alpha}_1 = -0.4x + 0.7$, and that v diverges driven by (2.2b).

https://doi.org/10.1017/S0956792524000329 Published online by Cambridge University Press

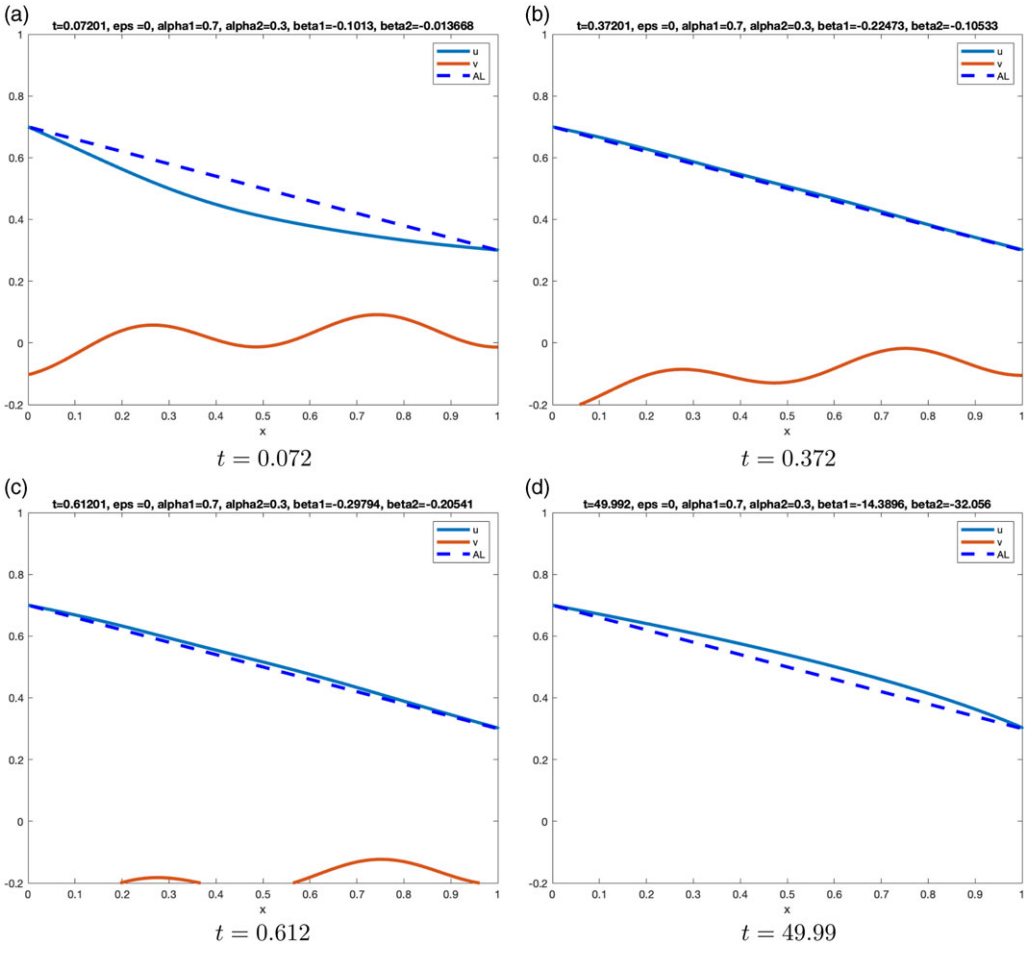

Figure 7. *Solution of (2.2) with* $\alpha_1 \to \bar{\alpha}_1 \neq \bar{\alpha}_2 \leftarrow \alpha_2$.

5.3. Convergence to time-periodic states

We study the dynamical behaviour of the solution with time-periodic boundary conditions for the following cases.

Case 1: $\boxed{\alpha_1 = \alpha_2, \beta_1 = \beta_2, \varepsilon > 0}$

We observe that the solution converges to a time-periodic state with the same exact period as the one of the boundary data.

For the simulations in Figure 8, we have chosen $\alpha_1 = 0.3 + 0.1 \sin(20\pi t) = \alpha_2$ and $\beta_1 = 0.7 + 0.1 \sin(20\pi t) = \beta_2$. We have used $\varepsilon = 0.7$. We observe that the time periodicity of the boundary data ($T = 1/10$) is induced in the stable time-periodic state with the same period.

Case 2: $\boxed{\alpha_1 \neq \alpha_2, \beta_1 \neq \beta_2, \varepsilon > 0}$

We observe that the solution converges to a time-periodic state whose period is the least common multiple of the periods of the boundary data.

For the simulations in Figure 9, we have chosen $\alpha_1 = 0.3 + 0.1 \sin(20\pi t)$, $\alpha_2 = 0.3 + 0.1 \sin(40\pi t)$ and $\beta_1 = 0.7 + 0.1 \sin(20\pi t)$, $\beta_2 = 0.7 + 0.1 \sin(40\pi t)$, and for the ones in Figure 10 we have chosen $\alpha_1 = 0.3 + 0.1 \sin(\pi t)$, $\alpha_2 = 0.3 + 0.1 \sin(\frac{2}{3}\pi t)$ and $\beta_1 = 0.7 + 0.1 \sin(\pi t)$, $\beta_2 = 0.7 + 0.1 \sin(\frac{2}{3}\pi t)$. In both cases, we use $\varepsilon = 0.7$ for the chemical diffusivity coefficient. We observe that the solution converges

https://doi.org/10.1017/S0956792524000329 Published online by Cambridge University Press

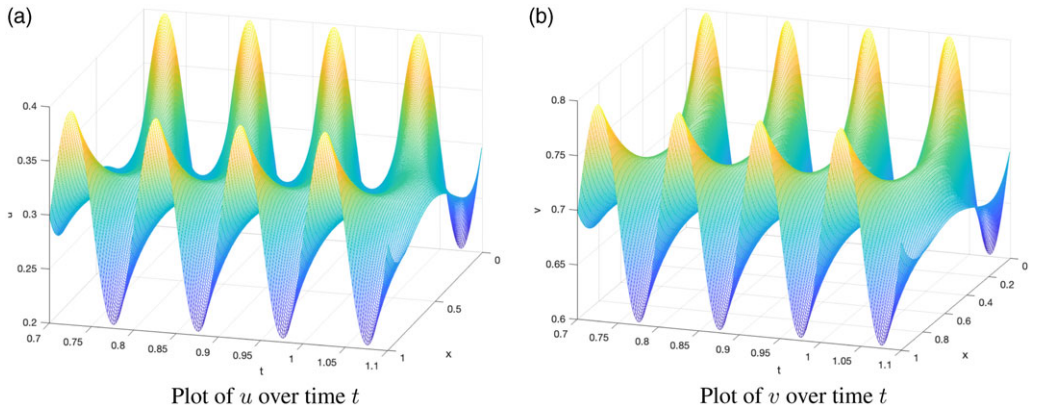

Figure 8. *Induced time-periodic state on solution of (2.1) with* $T = 1/10$ *for* $\alpha_1 = \alpha_2$, $\beta_1 = \beta_2$, $\varepsilon > 0$.

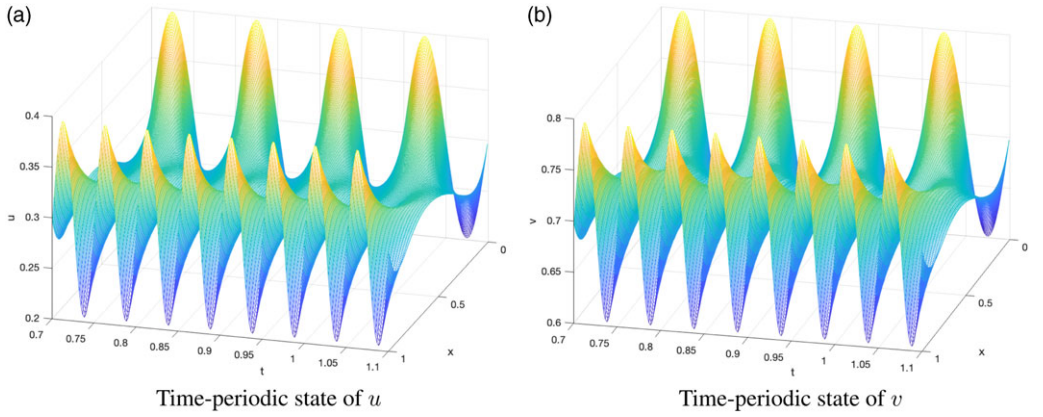

Figure 9. *Induced time-periodic state on solution of (2.1) with* $T = 1/10$ *for* $\alpha_1 \neq \alpha_2$, $\beta_1 \neq \beta_2$, $\varepsilon > 0$.

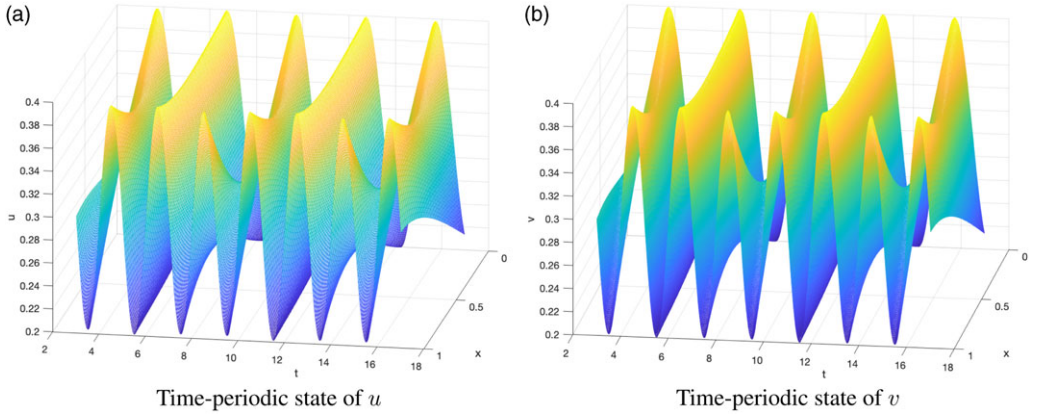

Figure 10. *Induced time-periodic state on solution of (2.1) with* $T = 6$ *for* $\alpha_1 \neq \alpha_2$, $\beta_1 \neq \beta_2$, $\varepsilon > 0$.

https://doi.org/10.1017/S0956792524000329 Published online by Cambridge University Press

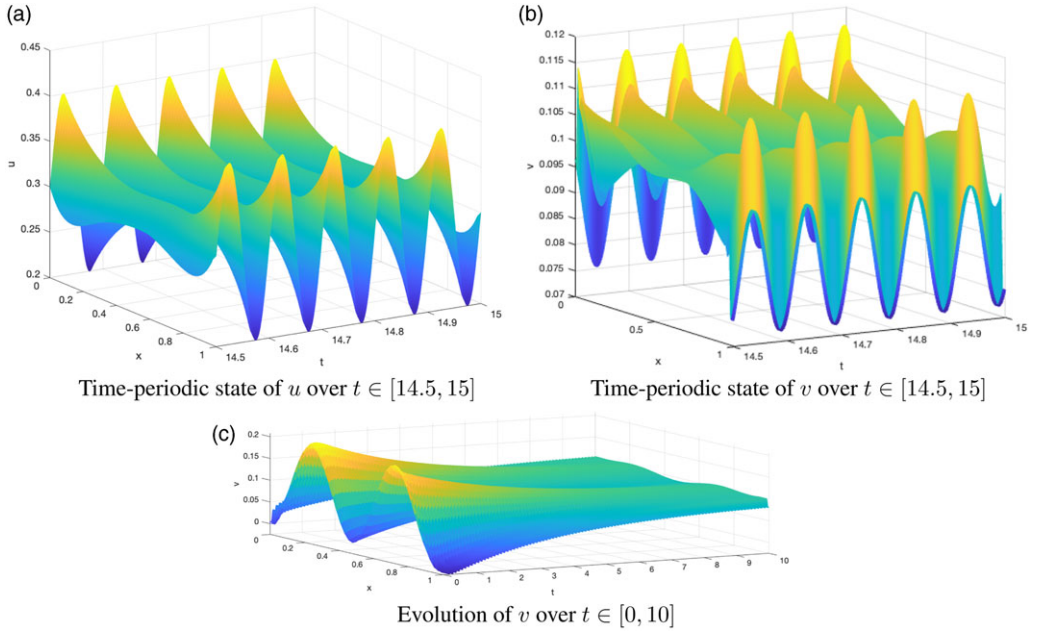

Figure 11. *Induced time-periodic state on solution of (2.1) with* $T = 1/10$ *for* $\alpha_1 = \alpha_2, \varepsilon = 0$.

to a time-periodic state whose period is the least common multiple of the periods of the boundary data ($T = 1/10$ for the first one and $T = 6$ for the second one). Figures 9a and 9b, and 10a and 10b show the evolution of both u and v over space and time for both cases.

Case 3: $\boxed{\alpha_1 = \alpha_2, \varepsilon = 0}$

We observe that the solution converges to a time-periodic state with the same period as that of the boundary data.

For the simulations in Figure 11, we have chosen $\alpha_1 = 0.3 + 0.1 \sin(20\pi t) = \alpha_2$. We observe that the time periodicity ($T = 1/10$) of the boundary data is induced in the time-periodic state. However, the solution v, in contrast with Case 1 in this section, takes a longer time to converge to the time-periodic state (see Figure 8b and Figures 11b–11c).

Case 4: $\boxed{\alpha_1 \neq \alpha_2, \varepsilon = 0}$

We observe that the time periodicity of the boundary data induces a time-periodic state of the solution u. When the periods of the boundary data are different, the solution picks up the least common multiple of the periods of the boundary data. Solution v will converge to a time-periodic state if the non-periodic parts of α_1 and α_2 are equal. However, in any other case, v will diverge as in Section 5.2, Case 3.

For the simulations in Figure 12, we have chosen $\alpha_1 = 0.3 + 0.1 \sin(20\pi t)$ and $\alpha_2 = 0.3 + 0.1 \sin(40\pi t)$. Figure 12a shows the induced time-periodic state of the solution u from the boundary data. In this case, the period induced ($T = 1/10$) is the least common multiple of the periods of the boundary data. Again, comparing Figures 12b–12c with Figure 9b, we see that it take solution v a longer time to converge to the time-periodic state.

6. Conclusion

We have studied the dynamical behaviour of classical solutions to the system of balance laws (1.3) with $\chi\mu > 0$, derived from the Keller–Segel type model of chemotaxis with logarithmic sensitivity (1.2), on a finite interval subject to time-dependent Dirichlet-type boundary conditions. For the model with

https://doi.org/10.1017/S0956792524000329 Published online by Cambridge University Press

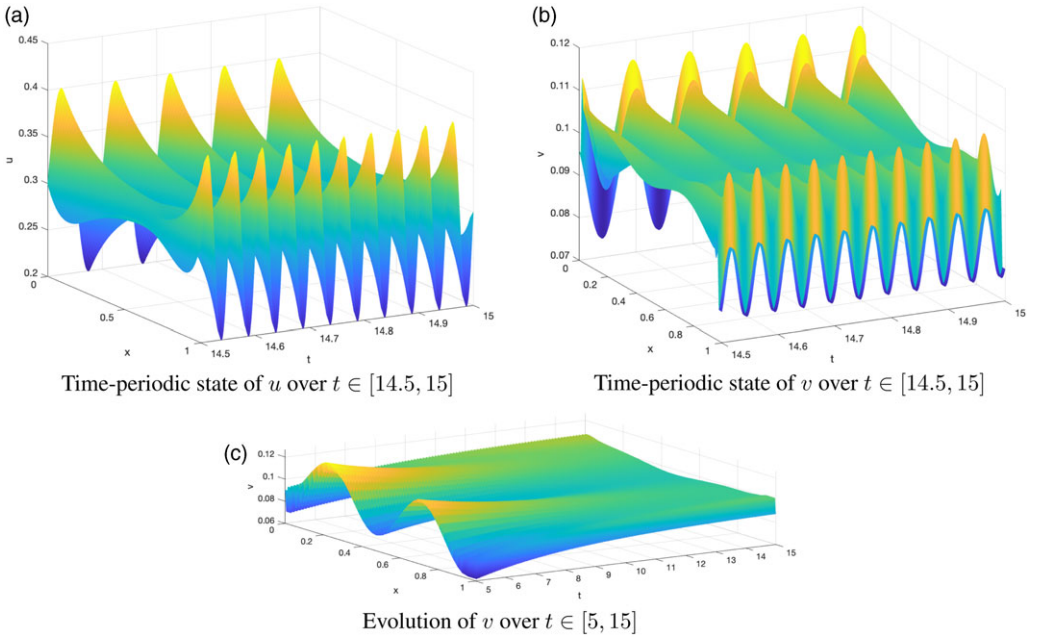

Figure 12. *Induced time-periodic state on solution of (2.2) with* $T = 1/10$ *for* $\alpha_1 \neq \alpha_2, \varepsilon = 0$.

$\varepsilon > 0$, it is shown that under the assumptions (2.6) and (2.7), classical solutions are globally well-posed and the perturbations around the reference profiles interpolating the boundary data converge to zero as time goes to infinity. There is no smallness restriction on the strength of the initial perturbations (see Theorem 2.1). This result generalises previous ones in the sense that the values of the function v at the endpoints of the spatial interval are allowed to be different at any time. When $\varepsilon = 0$, similar results are obtained, except in this case, the steady state of v is given by its initial average over the spatial interval (see Theorem 2.2).

Numerically, we have seen that by keeping the asymptotic convergence of the boundary data while relaxing the assumptions of Theorems 2.1 and 2.2, the solutions still converge to steady states, except in the case of zero chemical diffusion and unequal end-states of the boundary data for u, in which v diverges. For convergent solutions, when the end-states of the boundary data of u and/or v are different, the steady states of the solutions are non-trivial functions of x and are different from the linear profiles interpolating the corresponding end-states of the boundary data. On the other hand, when the boundary data are periodic in time, the periodicity of the boundary functions will induce time-periodic states of the solutions, except when there is no chemical diffusivity and the non-periodic parts of α_1 and α_2 are different. When the solutions converge to time-periodic states, the time-periodic states pick up the least common multiple of the periods of the boundary data.

The model considered in this article has been utilised to examine the role of protease inhibitors in the initiation of angiogenesis [21], which can be potentially linked to cancer treatments, such as chemotherapy. This work investigates how the dynamic input on the boundary of the spatial domain affects the behaviour of the solution in the interior of the domain. Given the time-dependent nature of cancer therapy, such as drug delivery, we believe that when this work can be verified experimentally, it will help provide meaningful insights into the design of effective therapeutic strategies for cancer patients. For example, our numerical simulations indicate that the time periodicity of the boundary data can be induced into the solution, and that the solution picks up the least common multiple of the boundary periods. This suggests that when a drug or chemical is periodically injected into the surrounding of a tumour near its boundary, one could make quantitative predictions (with a certain degree of confidence)

https://doi.org/10.1017/S0956792524000329 Published online by Cambridge University Press

of the time-periodic nature of the key quantities (e.g. cancer cells, drug concentration) inside of the tumour tissue, whose measurements are usually technically unfeasible. The predictions then could be combined with clinical data to evaluate the efficiency of drug delivery systems.

On the other hand, several of the numerical results observed in this article still remain to be proved analytically. For example, whether the matching boundary conditions for the function u can be relaxed so that similar results as Theorems 2.1 and 2.2 can be obtained (see Remark 2.3). Another direction of future exploration is the dynamical behaviour of the appended model with logistic growth in the u-equation. Because of the enhanced dissipation mechanism induced by logistic damping, the chemotaxis growth model may give us a definite answer to the preceding question.

Acknowledgements. The authors would like to thank Dr. Ricardo Cortez for the guidance in the numerical simulations, and Dr. Sujit S. Datta for the helpful conversations.

Financial Support. The research of K. Zhao was partially supported by the Simons Foundation's Collaboration Grant for Mathematicians No. 413028. The research of P. Fuster Aguilera was partially supported by the National Science Foundation's MPS-Ascend Postdoctoral Fellowship No. 2316699.

Competing interests. The authors declare none.

References

[1] Adler, J. (1966) Chemotaxis in bacteria. *Science* **153**(3737), 708–716.
[2] Aguilera, P. F., Martinez, V. & Zhao, K. (2023). A PDE model for chemotaxis with logarithmic sensitivity and logistic growth, Contemporary Research in Mathematical Biology: Modeling, Computation and Analysis. *Contemporary Mathematics and Its Applications: Monographs, Expositions and Lecture Notes*. in press. World Scientific.
[3] Bellomo, N., Bellouquid, A., Tao, Y. & Winkler, M. (2015) Toward a mathematical theory of Keller-Segel models of pattern formation in biological tissues. *Math. Models Methods Appl. Sci* **25**(09), 1663–1763.
[4] Carrillo, J., Li, J. & Wang, Z. (2021) Boundary spike-layer solutions of the singular Keller-Segel system: Existence and stability,. *Proc. London Math. Soc* **122**(1), 42–68.
[5] Chae, M. & Choi, K. (2020) Nonlinear stability of planar traveling waves in a chemotaxis model of tumor angiogenesis with chemical diffusion. *J. Differ. Equ* **268**(7), 3449–3496.
[6] Chae, M., Choi, K., Kang, K. & Lee, J. (2018) Stability of planar traveling waves in a Keller–Segel equation on an infinite strip domain. *J. Differ. Equ* **265**(1), 237–279.
[7] Choi, K., Kang, M., Kwon, Y. & Vasseur, A. (2020) Contraction for large perturbations of traveling waves in a hyperbolic–parabolic system arising from a chemotaxis model. *Math. Models Methods Appl. Sci* **30**(02), 387–437.
[8] Deng, C. & Li, T. (2014) Well-posedness of a 3D parabolic–hyperbolic Keller–Segel system in the Sobolev space framework. *J. Differ. Equ.* **257**(5), 1311–1332.
[9] Feng, Z., Xu, J., Xue, L. & Zhao, K. (2021) Initial and boundary value problem for a system of balance laws from chemotaxis: Global dynamics and diffusivity limit. *Ann. Appl. Math* **37**(1), 61–110.
[10] Fontelos, M., Friedman, A. & Hu, B. (2002) Mathematical analysis of a model for the initiation of angiogenesis. *SIAM J. Math. Anal* **33**(6), 1330–1355.
[11] Guo, J., Xiao, J., Zhao, H. & Zhu, C. (2009) Global solutions to a hyperbolic–parabolic coupled system with large initial data. *Acta Math. Sci. Ser. B (Engl. Ed.)* **29**, 629–641
[12] Hillen, T. & Painter, K. (2009) A users guide to PDE models for chemotaxis. *J. Math. Biol* **58**(1-2), 183–217.
[13] Horstmann, D. (2003) From 1970 until present: The Keller-Segel model in chemotaxis and its consequences I, Jahresber. *Dtsch. Math.-Ver* **105**, 103–165, 2003
[14] Hou, Q., Liu, C., Wang, Y. & Wang, Z. (2018) Stability of boundary layers for a viscous hyperbolic system arising from chemotaxis: One dimensional case. *SIAM J. Math. Anal* **50**(3), 3058–3091.
[15] Hou, Q. & Wang, Z. (2019) Convergence of boundary layers for the Keller–Segel system with singular sensitivity in the half-plane. *J. Math. Pures. Appl* **130**, 251–287.
[16] Hou, Q., Wang, Z. & Zhao, K. (2016) Boundary layer problem on a hyperbolic system arising from chemotaxis. *J. Differ. Equ* **261**(9), 5035–5070.
[17] Keller, E. & Segel, L. (1970) Initiation of slime mold aggregation viewed as an instability. *J. Theor. Biol* **26**(3), 399–415.
[18] Keller, E. & Segel, L. (1971) Model for chemotaxis. *J. Theor. Biol* **30**(2), 225–234.
[19] Keller, E. & Segel, L. (1971) Traveling bands of chemotactic bacteria: a theoretical analysis. *J. Theor. Biol* **26**(2), 235–248.
[20] Levine, H. & Sleeman, B. (1997) A system of reaction diffusion equations arising in the theory of reinforced random walks. *SIAM J. Appl. Math* **57**(3), 683–730.
[21] Levine, H., Sleeman, B. & Nilsen-Hamilton, M. (2000) A mathematical model for the roles of pericytes and macrophages in the initiation of angiogenesis I. the role of protease inhibitors. *Math. Biosci* **168**(1), 77–115.
[22] Li, D., Pan, R. & Zhao, K. (2015) Quantitative decay of a one-dimensional hybrid chemotaxis model with large data. *Nonlinearity* **28**(7), 2181–2210.

[23] Li, H. & Zhao, K. (2015) Initial-boundary value problems for a system of hyperbolic balance laws arising from chemotaxis. *J. Differ. Equ.* **258**(2), 302–338.
[24] Li, J., Li, T. & Wang, Z.-A. (2014) Stability of traveling waves of the Keller–Segel system with logarithmic sensitivity. *Math. Models Methods Appl. Sci* **24**(14), 2819–2849.
[25] Li, T., Pan, R. & Zhao, K. (2012) Global dynamics of a hyperbolic–parabolic model arising from chemotaxis. *SIAM J. Appl. Math* **72**(1), 417–443.
[26] Li, T. & Suen, A. (2015) Existence of intermediate weak solution to the equations of multi-dimensional chemotaxis systems. *Disc. Conti. Dyn. Syst* **36**(2), 861–875.
[27] Li, T., Wang, D., Wang, F., Wang, Z. & Zhao, K. (2021) Large time behavior and diffusion limit for a system of balance laws from chemotaxis in multi-dimensions. *Comm. Math. Sci* **19**(1), 229–272.
[28] Martinez, V., Wang, Z. & Zhao, K. (2018) Asymptotic and viscous stability of large-amplitude solutions of a hyperbolic system arising from biology. *Indiana Univ. Math. J* **67**(4), 1383–1424.
[29] Othmer, H. & Stevens, A. (1997) Aggregation, blowup and collapse: The ABC's of taxis in reinforced random walks. *SIAM J. Appl. Math* **57**(4), 1044–1081.
[30] Patlak, C. (1953) Random walk with persistence and external bias. *Bull. Math. Biophys* **15**(3), 311–338.
[31] Peng, H. & Wang, Z. (2018) Nonlinear stability of strong traveling waves for the singular Keller–Segel system with large perturbations. *J. Diff. Equ* **265**(6), 2577–2613.
[32] Peng, H., Wang, Z., Zhao, K. & Zhu, C. (2018) Boundary layers and stabilization of the singular Keller-Segel system. *Kinet. Relat. Models* **11**(5), 1085–1123.
[33] Rebholz, L., Wang, D., Wang, Z., Zerfas, C. & Zhao, K. (2019) Initial boundary value problems for a system of parabolic conservation laws arising from chemotaxis in multi-dimensions. *Discrete Contin. Dyn. Syst. A* **39**, 3789–3838
[34] Shizuta, Y. & Kawashima, S. (1985) Systems of equations of hyperbolic-parabolic type with applications to the discrete Boltzmann equation. *Hokkaido Math. J* **14**(2), 249–275.
[35] Tao, Y., Wang, L. & Wang, Z. (2013) Large-time behavior of a parabolic-parabolic chemotaxis model with logarithmic sensitivity in one dimension. *Disc Cont. Dyn. Syst., Ser. B* **18**, 821–845
[36] Teleanu, R.I., Chircov, C., Grumezescu, A.M. &Teleanu, D.M. (2019) Tumor angiogenesis and anti-angiogenic strategies for cancer treatment. *J. Clin. Med.* **9**(1), 84.
[37] Wang, D., Wang, Z. & Zhao, K. (2021) Cauchy problem of a system of parabolic conservation laws arising from the singular Keller-Segel model in multi-dimensions. *Indiana Univ. Math. J* **70**(1), 1–47.
[38] Wang, Z. (2013) Mathematics of traveling waves in chemotaxis. *Disc. Cont. Dyn. Syst. Ser. B* **18**, 601–641
[39] Wang, Z. & Zhao, K. (2013) Global dynamics and diffusion limit of a parabolic system arising from repulsive chemotaxis. *Commun. Pure Appl. Anal* **12**, 3027–3046
[40] Zeng, Y. (2017) Global existence theory for general hyperbolic/parabolic balance laws with application. *J. Hyper. Diff. Equ* **14**(02), 359–391.
[41] Zeng, Y. (2018) L^p decay for general hyperbolic/parabolic systems of balance laws. *Disc. Conti. Dyn. Syst* **38**, 363–396
[42] Zeng, Y. (2019) Hyperbolic-parabolic balance laws: Asymptotic behavior and a chemotaxis model. *Comm. Appl. Anal* **23**, 209–232
[43] Zeng, Y. (2022) Nonlinear stability of diffusive contact wave for a chemotaxis model. *J. Differ. Equ* **308**, 286–326.
[44] Zeng, Y. & Zhao, K. (2019) On the logarithmic Keller-Segel-Fisher/KPP system. *Disc. Cont. Dyn. Syst* **39**(9), 5365–5402.
[45] Zeng, Y. & Zhao, K. (2020) Erratum to "Optimal decay rates for a chemotaxis model with logistic growth, logarithmic sensitivity and density-dependent production/Consumption rate" [J. Differential Equations (2020) 1379-1411]. *J. Differ. Equ* **269**, 6359–6363.
[46] Zeng, Y. & Zhao, K. (2020) Optimal decay rates for a chemotaxis model with logistic growth, logarithmic sensitivity and density-dependent production/consumption rate. *J. Differ. Equ* **268**(4), 1379–1411.
[47] Zeng, Y. & Zhao, K. (2022) Asymptotic behavior of solutions to a chemotaxis-logistic model with transitional end-states. *J. Differ. Equ* **336**, 1–43.
[48] Zhang, M. & Zhu, C. (2006) Global existence of solutions to a hyperbolic–parabolic system. *Proc. Amer. Math. Soc* **135**(04), 1017–1027.
[49] Zhu, N., Liu, Z., Martinez, V. & Zhao, K. (2018) Global Cauchy problem of a system of parabolic conservation laws arising from a Keller-Segel type chemotaxis model. *SIAM J. Math. Anal* **50**(5), 5380–5425.
[50] Zhu, N., Liu, Z., Wang, F. & Zhao, K. (2021) Asymptotic dynamics of a system of conservation laws from chemotaxis,. *Disc. Cont. Dyn. Syst* **41**(2), 813–847.

Cite this article: Fuster Aguilera P. and Zhao K. Dynamical behaviour of a logarithmically sensitive chemotaxis model under time-dependent boundary conditions. *European Journal of Applied Mathematics*, https://doi.org/10.1017/S0956792524000329